Adaptive Tracking Controller for Real-Time Hybrid Simulation

Alejandro Palacio-Betancur
University of Kentucky, alejandro.palacio@uky.edu
Author ORCID Identifier:
https://orcid.org/0000-0003-3189-3406
Digital Object Identifier: https://doi.org/10.13023/etd.2020.318

STUDENT AGREEMENT:

I represent that my thesis or dissertation and abstract are my original work. Proper attribution has been given to all outside sources. I understand that I am solely responsible for obtaining any needed copyright permissions. I have obtained needed written permission statement(s) from the owner(s) of each third-party copyrighted matter to be included in my work, allowing electronic distribution (if such use is not permitted by the fair use doctrine) which will be submitted to UKnowledge as Additional File.

I hereby grant to The University of Kentucky and its agents the irrevocable, non-exclusive, and royalty-free license to archive and make accessible my work in whole or in part in all forms of media, now or hereafter known. I agree that the document mentioned above may be made available immediately for worldwide access unless an embargo applies.

I retain all other ownership rights to the copyright of my work. I also retain the right to use in future works (such as articles or books) all or part of my work. I understand that I am free to register the copyright to my work.

REVIEW, APPROVAL AND ACCEPTANCE

The document mentioned above has been reviewed and accepted by the student's advisor, on behalf of the advisory committee, and by the Director of Graduate Studies (DGS), on behalf of the program; we verify that this is the final, approved version of the student's thesis including all changes required by the advisory committee. The undersigned agree to abide by the statements above.

<div align="right">

Alejandro Palacio-Betancur, Student

Dr. Mariantonieta Gutierrez Soto, Major Professor

Dr. Timothy Taylor, Director of Graduate Studies

</div>

ADAPTIVE TRACKING CONTROLLER FOR REAL-TIME HYBRID SIMULATION

THESIS

A thesis submitted in partial
fulfillment of the requirements for
the degree of Master of Science in
Civil Engineering in the College of
Engineering at the University of
Kentucky

By
Alejandro Palacio-Betancur
Lexington, Kentucky

Director: Dr. Mariantonieta Gutierrez Soto,
Assistant Professor of Civil Engineering
Lexington, Kentucky 2020

ABSTRACT

ADAPTIVE TRACKING CONTROLLER FOR REAL-TIME HYBRID SIMULATION

Real-time hybrid simulation (RTHS) is a versatile and cost-effective testing method for studying the performance of structures subjected to dynamic loading. RTHS decomposes a structure into partitioned physical and numerical sub-structures that are coupled together through actuation systems. The sub-structuring approach is particularly attractive for studying large-scale problems since it allows for setting up large-scale structures with thousands of degrees of freedom in numerical simulations while specific components can be studied experimentally.The actuator dynamics generate an inevitable time delay in the overall system that affects the accuracy and stability of the simulation. Therefore, developing robust tracking control methodologies are necessary to mitigate these adverse effects. This research presents a state of the art review of tracking controllers for RTHS, and proposes a Conditional Adaptive Time Series (CATS) compensator based on the principles of the Adaptive Time Series compensator (ATS). The accuracy of the proposed controller is evaluated with a benchmark problem of a three-story building with a single degree of freedom (SDOF) in a realistic virtual RTHS (vRTHS). In addition, the accuracy of the proposed method is evaluated for seven numerical integration algorithms suitable for RTHS.

KEYWORDS: Real-Time Hybrid Simulation, Time delay, Adaptive time delay compensation, Explicit numerical integration

Author's signature: Alejandro Palacio-Betancur

Date: April 20, 2020

ADAPTIVE TRACKING CONTROLLER FOR REAL-TIME HYBRID
SIMULATION

By

Alejandro Palacio-Betancur

Director of Thesis: Mariantonieta Gutierrez Soto

Director of Graduate Studies: Timothy Taylor

Date: April 20, 2020

To my parents Aracelly and Leonel

ACKNOWLEDGMENTS

Primarily I would like to express my gratitude to my advisor Dr. Mariantonieta Gutierrez Soto for her support and valuable advice throughout this process. She consistently steered me in the right direction when I needed it, I am very thankful for that. Her knowledge and leadership helped me grow as a professional and as a person.

I would also like to acknowledge Dr. Issam E. Harik from the department of Civil Engineering and Dr. Bruce L. Walcott from the department of Electrical Engineering as members of the evaluation committee. I am grateful for their guidance and valuable feedback during this project.

Then I would like express my gratitude to my parents and my sister for providing me with their support and encouragement throughout this process. This accomplishments would not have been possible without them. Thank you sincerely.

TABLE OF CONTENTS

LIST OF TABLES

ABBREVIATIONS

A/D	Analog to digital
AFP	Adaptive Forward Predictor
ATS	Adaptive time series
AXR	Autoregressive with Exogenous Input
CATS	Conditional adaptive time series
CDM	Central Difference Method
CSI	Control-structure interaction
D/A	Digital to analog
DFC	Derivative feed-forward
DOF	Degree of freedom
dRTHS	Distributed RTHS
D-RTHS	Dual computer RTHS
EFC	Equivalent Force Control
FE	Finite element
FEI	Frequency Evaluation Index
FIR	Finite Impulse Response
gRTHS	Geotechnical RTHS
HIL	Hardware-In-The-Loop
HS	Hybrid Simulation
IAFP	Improved AFP
IIR	Infinite Impulse Response
LQE	Linear Quadratic Estimation
LQG	Linear Quadratic Gaussian
LS	Least square algorithm
LTR	Loop Transfer Recovery
maRTHS	Multi-Axial RTHS
MCS	Minimal Control Synthesis
MCSmd	Numerical model Substructure Minimal Control Synthesis
MDOF	Multiple Degree Of Freedom
MIMO	Multi-Input Multi-Output
NRMS	Normalized root mean square
PHIL	Power Hardware-In-The-Loop
PID	Proportional-Integral-Derivative
PLC	Phase-Lead Compensator
PsD	Pseudodynamic testing
PSI	Predictive stability indicator
RFC	Restoring Force Compensator
RLQG	Robust Linear Quadratic Gaussian

SYMBOLS

$\ddot{x}_g$	Ground acceleration
$\ddot{\mathbf{x}}$	Acceleration vector
$\dot{\mathbf{x}}$	Relative velocity vector
$\mathbf{A}_k$	Adaptive compensation parameters vector at time step
$\mathbf{C_e}$	Experimental substructure damping matrix
$\mathbf{C_n}$	Numerical substructure damping matrix
$\mathbf{C_r}$	Reference structure damping matrix
$\mathbf{f_e}$	Feedback force vector
$\mathbf{K_e}$	Experimental substructure stiffness matrix
$\mathbf{K_n}$	Numerical substructure stiffness matrix
$\mathbf{K_r}$	Reference structure stiffness matrix
$\mathbf{M_e}$	Experimental substructure mass matrix
$\mathbf{M_n}$	Numerical substructure mass matrix
$\mathbf{M_r}$	Reference structure mass matrix
$\mathbf{P}_k$	inverse correlation matrix at time step
$\mathbf{U_c}$	Compensated target displacement vector
$\mathbf{X_m}$	Measured state matrix
$\mathbf{x_m}$	Measured displacement vector
$\mathbf{x}$	Relative displacement vector
$\mathbf{x}^{(j)}$	j-th element of the relative displacement vector
$\mathbf{x}_r^{(j)}$	j-th element of the reference structure displacement
$\mathbf{y_n}$	Numerical substructure output vector
a_2	Parameter of the transfer system associated with the actuator
a_3	Parameter of the transfer system associated with the actuator
a_i	coefficients of polynomial extrapolation
a_m	Inverse compensator pole
b_m	Low frequency gain
A_k	Amplitude error at step
c_e	Damping of the experimental substructure

$c_e q$	Equivalent negative damping
c_v	virtual damping
C_p	Proportional gain
C_v	Velocity gain
f_e	Measured force
G_{ff}	Feed-forward transfer function
G_P	Control plant transfer function
G_{PID}	PID transfer function
G_C	Controller transfer function
H_f	Low pass filter transfer function
I_a	Amplitud indicator
I_d	Tracking indicator
k	Discrete sample time
k_a	Amplitude error correction
k_e	Stiffness of the experimental substructure
k_{est}	Initial estimation of the proportional gain
k_{ff}	Feed-forward gain
k_i	Integral gain
k_m	Model-based compensator gain
k_p	Proportional gain
k_v	Virtual stiffness
K_m	Adaptive feed-forward gain
K_r	Adaptive feedback gain
m	Length of the measurement vector after decimation process
m_e	Mass of the experimental substructure
n	Order of the polynomial expression
p_i	Transfer function poles
q	Number of previous states of the measured displacement
s	Laplace operator
S_o	Spectral Intensity
S_s	Sampling size of the compensator
t	Time variable
T_s	Sampling time
u	Actuator displacement command
u_k^*	Overcompensated displacement

v_i	Control output of rule i
W_1	Adaptive phase-lead parameter
W_2	Adaptive phase-lead parameter
$x_c^{(1)}$	Compensated target displacement of the first floor
x_m	Measured displacement
y_{G_C}	Command signal to the transfer system
y_{G_P}	Output vector of the control plant
α_{jk}	j-th adaptive compensation parameter at step k
β_1	Parameter of the transfer system associated with the servo-valve
β_2	Parameter of the transfer system associated with the servo-valve
γ	Column vector defined by spatial location of the interface DOF
λ	Forgetting factor of the RLS algorithm
$\mathbf{\Phi}$	Kalman Gain vector
ω_g	Ground frequency
τ	Actuator time-delay
τ_k	Actuator time-delay at step
τ_{cr}	Critical time-delay
ι	Influence vector
ζ_g	Ground damping ratio
$a_1\beta_0$	Parameter of the transfer system associated with the servo-valve

1 Introduction

1.1 General

An essential role in the design of structural systems is the performance evaluation of structures subjected to environmental loading such as earthquake and wind. The development of computer programs and the implementation of complex numerical models are useful tools for a preliminary study and design of structures. However, these are not always sufficient to fully understand the behavior of a structural system subjected to realistic loading conditions. The conventional approach for experimental testing is through the usage of shake tables or wind tunnels, but it has its limitations. First, the implicit financial burden to investigate structures at full-scale. Second, loading condition challenges for structures subjected to multiple hazards. The structure is often only subjected to single environmental load, *e.g.*, base excitation shake table or wind tunnel testing. Third, experimental facilities have limited space and capacity in their actuation systems; therefore, a large structure often will require size reduction that lead to scaling challenges. The extrapolation of results from the specimen to the full-scale is not always accurate due to nonlinearities in the structure or loading effects [1].

These challenges led to the development of alternative experimental methods, one of them is Hybrid Simulation (HS) [2]. In some engineering disciplines, this concept is also known as Hardware-In-the-Loop (HIL) and is used for studying dynamic systems such as large-scale power systems [3] and cruise control in autonomous ground vehicles [4]. This concept was first introduced in civil engineering as Pseudodynamic testing (PsD) [2]. PsD is an alternative to shake table testing because it decomposes a structure into physical and numerical sub-structures. Components of interest, or challenging modeling elements, can be selected as the physical sub-structure and the rest is modeled numerically. Fig. 1.1 shows a typical hybrid simulation of a building structure subjected to earthquake loading. Fig. 1.1(a) shows the actual system of a three-dimensional building structure equipped with three dampers subjected to earthquake loading. Fig. 1.1(b) shows the numerical and experimental substructures, where the 3D building structure is modeled numerically and the dampers are

setup for experimental testing. The numerical and experimental substructures are in a loop configuration interacting at the interface.
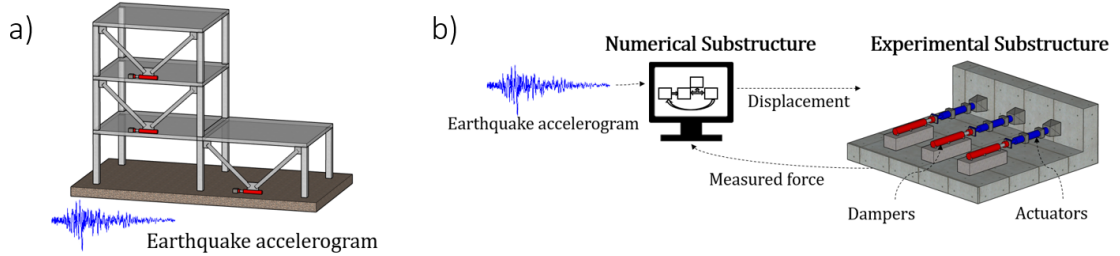
Figure 1.1: Hybrid simulation of a building structure subjected to earthquake loading (a) actual system (b) numerical and experimental substructures configuration

When the structure has velocity-dependent components such as damping devices, the test must be implemented in real-time due to the importance of time-dependent characteristics; this is known as Real-Time Hybrid Simulation (RTHS) [5]. Over the last decades, RTHS has improved due to frequent implementations of the method in the development of structural control strategies such as semi-active control of magneto-rheological damping devices [6]–[8], and passive control devices (e.g. viscous dampers [9] and elastomeric dampers[10]). RTHS has been used to study different loading conditions such as wind loads [11], [12] and wave loads [13], [14]. Methodologies for RTHS have challenges in the areas of computation and communication speed, numerical integration methods, stability assessment tools, control design, and actuator compensation. This research presents background on hybrid simulation and presents representative recent developments of control methodologies suitable for RTHS of building structures subjected to natural hazards with a focus on seismic loading.

1.2 Research objectives

The objectives of this research are:

- Introduce the concept of hybrid simulation from its origin and describes the differences between Hardware-in-the-loop (HIL), Pseudodynamic testing (PsD), and Real-Time Hybrid Simulation (RTHS)

- Present a state of the art review of recent papers published on developments of tracking control methodologies suitable for RTHS.

- Develop and use a tracking controller capable of mitigating errors generated by actuator delays in RTHS systems

- Investigate the accuracy and robustness of a proposed controller with a realistic vRTHS benchmark problem based on different performance criteria and different partitioning cases

- Evaluate the accuracy of numerical integration methods suitable for RTHS with ha realistic vRTHS benchmark problem

1.3   Overview of Thesis

This thesis focuses on the development of an accurate and robust tracking control algorithm suitable for several RTHS applications in Civil Engineering. To achieve this goal, it is important to understand that the implementation of RTHS as a testing method requires specialized knowledge in the areas of signal processing, control system design, and structural dynamics. Therefore, this research first contextualizes this testing method with other strategies implemented in previous decades, such as HIL and PsD, to understand requirements, capabilities, and key components involved in the process. This information provides the foundation for future research in RTHS of structures subjected to multiple hazards. Then, based on recent developments on time delay compensation, a new adaptive tracking controller is proposed and evaluated for structures subjected to seismic loading. To assess the accuracy of the proposed methodology, a vRTHS benchmark problem is implemented considering different partitioning cases to evaluate the versatility and robustness of the proposed scheme. In addition, another important component of RTHS is the behavior of the numerical structure that is usually obtained through numerical integration methods. This process needs to be achieved in short periods of time because the simulation is carried out in a time-step fashion. Thus, the proposed controller is also implemented with a series of explicit numerical integration methods proposed in the literature suitable for RTHS.

This thesis consists of five chapters, where the remaining four chapters are organized as follows:

- **Chapter 2** reviews background information on RTHS including the origin of the method, possible experimental setups, and developments of tracking control methodologies suitable for RTHS.

- **Chapter 3** presents the development and implementation of a new adaptive tracking controller called the Conditional Adaptive Time Series (CATS) controller. The proposed method is based on the principle of the ATS compensator and provides improvements in online parameter estimation and addresses issues related to simulations with large noise-to-signal ratio

- **Chapter 4** shows a comparative study of seven numerical integration methods with the vRTHS benchmark problem using the proposed CATS controller

- **Chapter 5** summarizes the findings and conclusions from this study, and makes recommendations for future research

2 Background

2.1 Hardware-In-the-Loop

Hybrid simulation was first developed in mechanical and aerospace engineering and is known as Hardware-In-the-Loop (HIL). It has been used for several decades in the design of control systems, and consists of testing a system divided into hardware and software components linked through an interface and subjected to design conditions, especially under extreme design conditions [15]. It can be subdivided according to: a) the speed required by the test (without time limitation, in real-time and faster than real-time) [15], and b) the components being simulated (signal, power and mechanical levels) [16]. It is considered a versatile, fast and cost effective alternative of design and development of control systems [17] if the coupling between physical and simulated components is addressed properly to guarantee synchronicity [18].

HIL has been extensively used in the automotive industry on the design of vehicle components (e.g. engines, suspension, braking systems) [15], [17] and examples of recent applications in different fields can be found in the literature. Luo *et al.* [19] proposed a stability analysis method for power hardware in the loop (PHIL) to study the impact of wind turbines on grid support. Andreev *et al.* [3] used PHIL for electric power systems to minimize inaccuracies created by analog simulators and errors created in the solution of the governing differential equation. Aziz *et al.* [20] developed a hybrid control method to improve control performance in power grids. The inner loop consists of a variable fuzzy logic controller and the outer loop is a genetic algorithm that optimizes its control parameters online. The authors tested the proposed method with a PHIL of a system with 12 generators, 49 transmissions lines and 37 load centers. Cale *et al.* [21] introduced a communication delay compensation strategy to improve accuracy in remotely connected HIL experiments, which are virtually connected circuits but physically separated over $100\,\mathrm{km}$. Yu *et al.* [22] studied a force and displacement compensation methodology for manipulator docking HIL to reduce dynamic response delay of motion simulation of on-orbit docking dynamics processes. Joshi [23] implemented HIL simulation to study longitudinal, lateral and supervisory control of autonomous ground vehicles.

2.2   Hybrid simulation

Previously known as Pseudo-dynamic testing (PsD), Hybrid Simulation (HS) was introduced in structural engineering in the 1960s by Hakuno *et al.* [2] and it was first implemented by Takanashi *et al.* [24] as an alternative dynamic testing to shake table testing. The idea was developed for a single degree of freedom (SDOF) system with time step explicit integration of the equation of motion in an extended time scale. The inertial forces and the damping of the structure are derived numerically and the physical model was subjected to these forces with a hydraulic actuator. The slow process allows the analysis of the response in each time step; however, this method is effective for structures without rate-dependent behavior because the forces are applied quasi-statically.

In order to carry out HS, the step-wise operation process was divided in two phases, a *pause* required for calculations and a *ramp period* to apply displacements [25]. This process allowed a degree of relaxation in the structure that induced errors in the simulation. This drawback was solved by the development of continuous PsD [26], where dynamic actuators followed the target displacement without motion discontinuity. Afterwards, sub-structuring was proposed to avoid complexity of experiments on large structures. It is required to build only elements of interest or elements which behavior is difficult to model numerically [27] (Fig. 1.1), and the number interaction points between numerical and physical substructures are known as the HS degrees of freedom (DOF). This led to simplified physical models with few actuators; however, other complex studies have been developed. Dhakal *et al.* [28] use bidirectional actuators to study the simultaneous bidirectional interaction effect of reinforced concrete piers subjected to earthquake loading. Obata and Goto [29] use multi-directional testing system with 6 DOF to load columns and bridge piers accurately combining bi-axial bending and axial loads during earthquake loading.

2.3   Real-Time Hybrid Simulation

HS of structures with rate-dependent components, such as damping devices for structural control, led to the introduction of fast PsD [5] where the time scale of the conventional PsD matches real-time simulation also known as Real-Time Hybrid Simulation (RTHS). The measured restoring force in the conventional HS is equivalent to the stiffness of the physical sub-structure due to the slow testing, but in

RTHS the inertial and damping forces of the physical substructure are also measured as restoring forces in order to study rate-dependent components. Researchers have developed different RTHS setups includes Real-Time Hybrid Simulation Table Test (RTHSTT), multi-axial Real-time Hybrid Simulation (maRTHS), geotechnical Real-Time Hybrid Simulation (gRTHS), Real-Time Aerodynamic Hybrid Simulation (RTAHS), Real-Time Hybrid Simulation of Ocean Structures (RTHSOS), distributed Real-Time Hybrid Simulation (dRTHS), dual target computers Real-Time Hybrid Simulation (D-RTHS), and virtual Real-Time Hybrid Simulation (vRTHS).

The first method variation was proposed using RTHS with shake tables to develop RTHSTT and study structures equipped with damping devices including Tuned Mass Dampers (TMD) [30]–[32] and active mass dampers [33]. The floor of the structure with damping system installation is built on the shake table and the rest of the building is modeled numerically as shown in Fig. 2.1. More recently, Schellenberg *et al.* [34] used RTHSTT to study mid-level isolation systems subjected to earthquake loading, where traditional base isolation systems are placed in a level different to the base of the building.
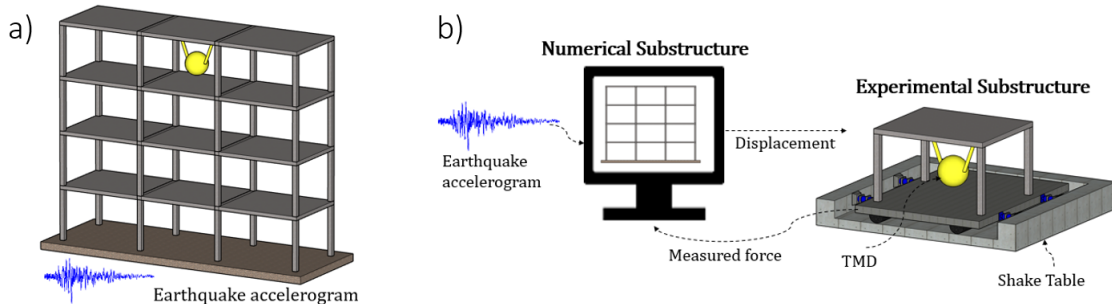
Figure 2.1: RTHSTT configuration (a) actual system (b) numerical and experimental substructures

In addition, there are simulations where the boundary between substructures has more than one DOF in the same location. This is called maRTHS and requires the coupling of several dynamic actuators in order to generate translational and rotational DOF as shown in Fig. 2.2. Fermandois *et al.* [35] developed a framework for maRTHS considering a multi-input, multi-output (MIMO) controller design to obtain accurate tracking displacement and noise reduction.
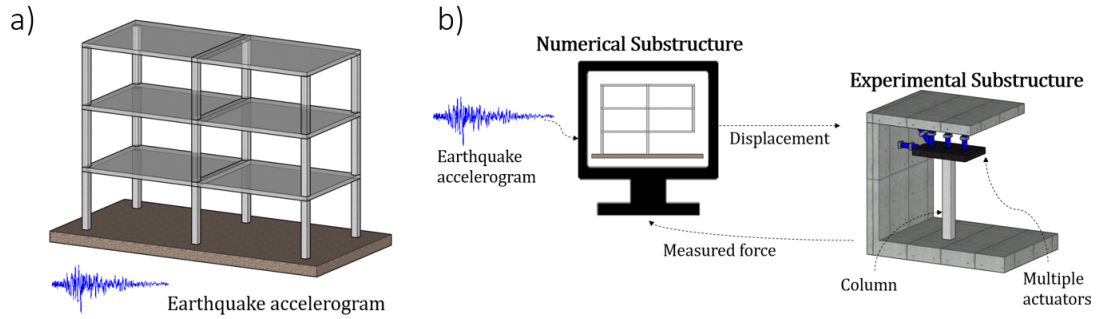
Figure 2.2: maRTHS configuration (a) actual system (b) numerical and experimental substructures

Further research led to the study of soil-structure interaction (SSI) with gRTHS. This can be achieved with a geotechnical laminar box and a shake table as shown in Fig. 2.3. Colletti [36] developed a framework for a full-scale laminar box gRTHS where the phenomena related to SSI can be isolated and quantified in order to carry out different dynamic testing conditions.
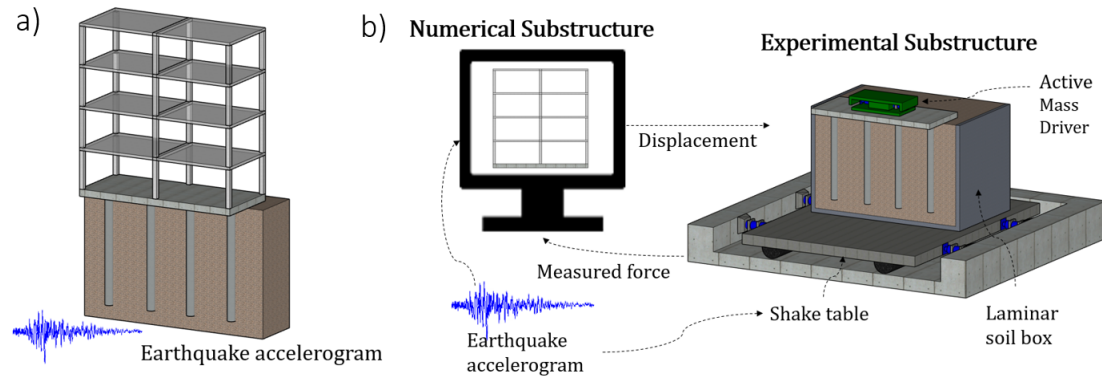
Figure 2.3: gRTHS configuration (a) actual system (b) numerical and experimental substructures

Moreover, structures subjected to wind loading can be studied with RTAHS. Wu and Song [11] introduced a methodology to implement RTAHS of tall buildings with dampers, where a rigid-body aeroelastic model of the building is placed in a wind tunnel to capture essential aerodynamic wind loads and aeroelastic effects, and a full-scale model of a damper is coupled to the structure through scaling conversion algorithms and an actuator control algorithm as shown in Fig. 2.4. Zhang *et al.* [12] applied RTAHS to study wind turbines equipped with tuned liquid dampers (TLD) where the numerical substructure is a 13 DOF aeroelastic model of the wind turbine

and the physical substructure is the full-scale TLD.
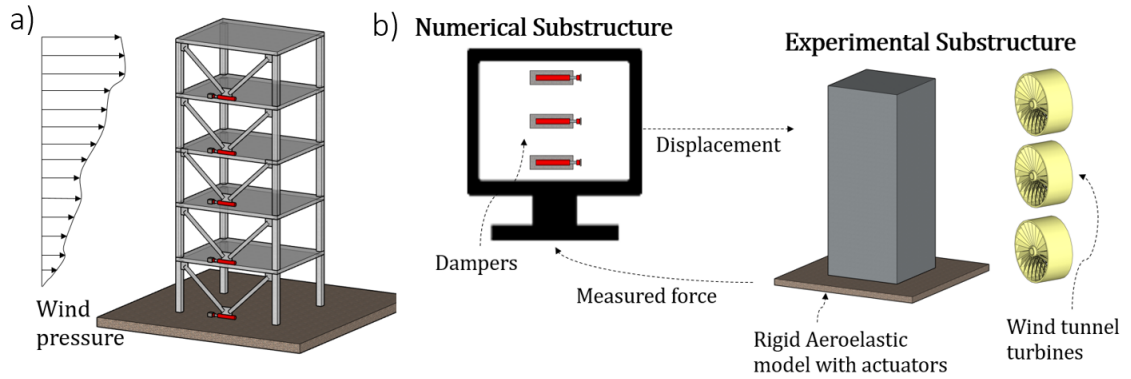
Figure 2.4: RTAHS configuration (a) actual system (b) numerical and experimental substructures

A current development allows the study of ocean structures subjected to wind and wave loads with RTHSOS [37]. Sauder *et al.* [13] proposed a testing setup to study a floating wind turbine as shown in Fig. 2.5 and Vilsen *et al.* [14] formulated a setup design process for RTHSOS with seven steps that addressess guidelines to analyze the accuracy of the simulation.
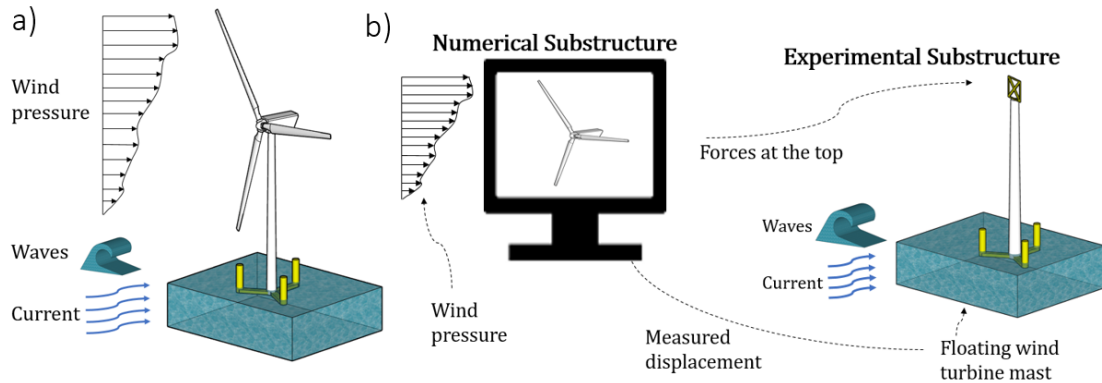
Figure 2.5: RTHSOS configuration (a) actual system (b) numerical and experimental substructures

The previously explained types of RTHS consist in variations of loading conditions; however, there are additional types that depend on variations in execution process. For example, dRTHS is the combination of laboratories resources as shown in Fig. 2.6 that allows the execution of complex experiments [38]. Li *et al.* [39] proposed a

framework to conduct dRTHS and evaluated the performance experimentally through a series of test at geographically separate facilities located at Purdue University in west Lafayette, Indiana, USA and University of Connecticut in Storrs, Connecticut, USA.
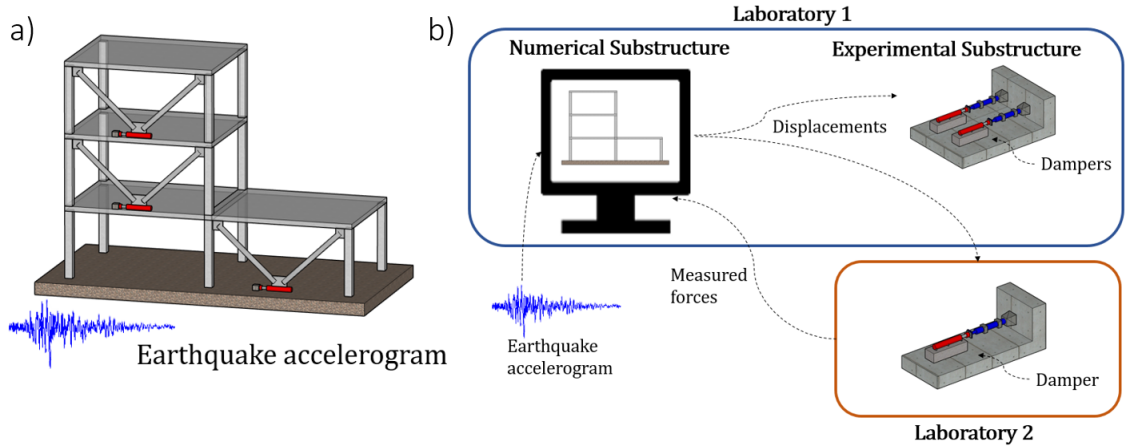
Figure 2.6: dRTHS configuration (a) actual system (b) numerical and experimental substructures

Another development is D-RTHS, it can improve the execution of complicated tasks that need to be carried out in short periods of time. The sampling frequency of RTHS may vary between $1024\,\mathrm{Hz}$ and $2048\,\mathrm{Hz}$; therefore, when structures with a many DOF are studied it becomes a challenging task. When dual target computers are used, the numerical substructure is solved in one computer with a desired time-step and the target displacement is obtained at sub-time steps through interpolation in the second computer as shown in Fig. 2.7. Lu *et al.* [40] modified D-RTHS by combining a sub-stepping technique and a multi-core parallel programming to provide a method for the calculation of numerical substructure in RTHS.

Another variation in execution is vRTHS, it is a useful tool for the development of control strategies or numerical integration methods. The components of the RTHS are modeled and the interaction between the substructures is taken into account [41], [42]. Silva *et al.* [43] developed a benchmark problem of a three-story frame structure that uses vRTHS for the investigation of tracking control methodologies for RTHS of a shear frame structure subjected to seismic loading.
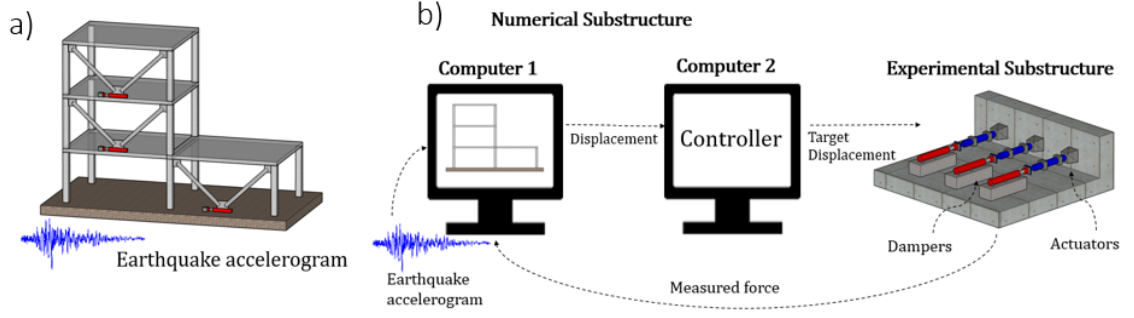
Figure 2.7: D-RTHS configuration (a) actual system (b) numerical and experimental substructures

2.4 RTHS of Structural Systems

The equation of motion of the reference structure shown in Fig. 1.1(a) is given by:

$$\mathbf{M_r}\ddot{\mathbf{x}} + \mathbf{C_r}\dot{\mathbf{x}} + \mathbf{K_r}\mathbf{x} = -\mathbf{M_r}\iota\ddot{x}_g \tag{2.1}$$

where $\mathbf{M_r}, \mathbf{C_r}, \mathbf{K_r}$ are the mass, damping and stiffness matrices of the reference structure, respectively. $\mathbf{x}, \dot{\mathbf{x}}, \ddot{\mathbf{x}}$ are the displacement, velocity and acceleration vectors of the reference structure, respectively. $\ddot{x}_g$ is the ground acceleration and ι is the influence coefficient vector.

The partitioning of the reference structure into numerical and experimental substructures leads to a partition of the matrices of the system, where $\mathbf{M_r} = \mathbf{M_e} + \mathbf{M_n}$, $\mathbf{K_r} = \mathbf{K_e} + \mathbf{K_n}$ and $\mathbf{C_r} = \mathbf{C_e} + \mathbf{C_n}$, the subscripts e and n refer to experimental and numerical substructures, respectively.

Therefore, the Eq. 3.1 is revised and the equation of motion of the system shown in Fig. 1.1(b) is formulated as:

$$\mathbf{M_n}\ddot{\mathbf{x}} + \mathbf{C_n}\dot{\mathbf{x}} + \mathbf{K_n}\mathbf{x} = -\mathbf{M_r}\iota\ddot{\mathbf{x_g}} - \mathbf{f_e} \tag{2.2}$$

where $\mathbf{f_e}$ is the feedback force vector, known as the restoring force vector, determined from the measured forces of the experimental substructure. The block diagram of a typical RTHS system is shown in Fig. 3.3. The ground acceleration $(\ddot{x}_g)$ and the feedback force vector $(\mathbf{f}_e)$ are the input to the numerical substructure, $\mathbf{x}_n$ is the output of the numerical substructure that may be used as the input to the control transfer function (G_c). The tracking controller generates the command signal $(\mathbf{u})$ to

the control plant (G_p), that consists of actuators and the experimental substructure. The sensors obtain the output vector $\mathbf{x}_{G_p}$ that contains the measured displacements $\mathbf{x}_m$, and the feedback force vector, $\mathbf{f}_e$.
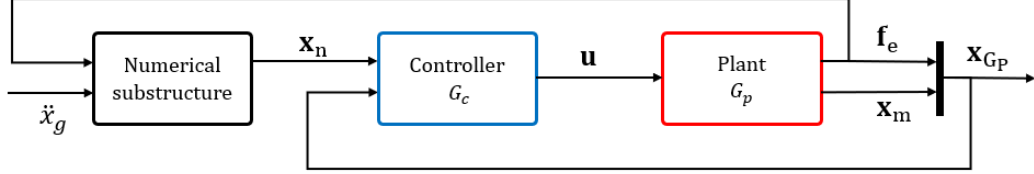
Figure 2.8: Block diagram of a typical RTHS

The solution of the equation of motion is obtained through numerical time-step explicit or implicit integration algorithms. The difference between these approaches is the information used to estimate displacement, velocity and acceleration of the DOF. Explicit integration obtains the response only with information from previous steps and implicit algorithms obtain the response based on current and previous steps. The former may be conditionally stable and the latter are unconditionally stable but require higher computational cost.

2.5 Control Methodologies for RTHS

The coupling between physical and numerical substructures generates challenges related to computational delays, signal transmission, instrument calibration and actuator delays [44]. Actuator delays have been identified as the most significant [45]. Hourichi *et al.* [46] showed that the actuator delay causes a counterclockwise hysteresis causing the total energy of the system to increase. This hysteresis is shown in the synchronized subspace plot where the target and measured displacement are compared exhibited in Fig. 2.9. The time delay can be interpreted as an equivalent negative damping $(c_{eq} = -k_e\tau)$, where k_e is the stiffness of a SDOF structure and τ is the time delay. If the negative damping is greater than the inherent structural damping, the simulation becomes difficult to execute because the response is unstable. The system's time delay when the simulation becomes unstable is called *critical time delay* and it can be estimated according to the partitioning choice of the reference structure [47]. Maghareh *et al.* [48] obtains the critical time delay using an eigenvalue problem deduced from the delay differential equation of the system. Gao et al. [49] quantifies the critical time delay using the linearized RTHS equations of motion for SDOF, and

Gao et al. [50] extended this study for MDOF systems. The estimated critical time delay can be used to determine the predictive stability and performance indicators for SDOF systems [51], [52] and MDOF systems [53]. This is useful when designing and assessing the sensitivity of an RTHS for a specific substructure configuration. Also, there are several error assessment measures for RTHS at a synchronization level between substructures and at a system level for global stability of the simulation [54].
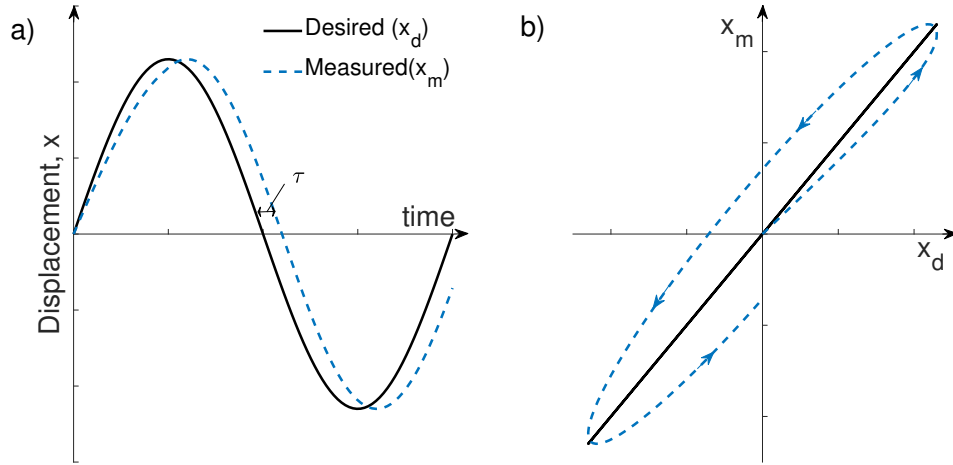
Figure 2.9: Effects of time delay on RTHS: a) Variation in displacement b) Synchronized subspace plot

The delay effects can be reduced when a time delay compensation method is implemented along with a servo-controller of the hydraulic actuator; however, the prediction of desired displacements in real-time is not a straightforward task. Hourichi *et al.* [46] used a polynomial extrapolation of the displacement but caused a virtual variation in stiffness and damping. This approach allowed RTHS of structures with higher stiffness and lower damping than the one studied by Nakashima *et al.* [5]; nevertheless, the stability of this approach is limited for structures with high-frequency response such as MDOF structures.

A robust and accurate time delay compensation is a key challenge for RTHS development. Researchers have studied methodologies based on constant time delay while others have studied variable time delay. The latter is a realistic approach to the dynamic behavior of actuators coupled with linear or nonlinear physical substructures.

Methodologies that investigate time delay in RTHS of structures subjected to seismic loading can be subdivided into polynomial extrapolation, phase-lead compensation, model-based compensation, derivative feed-forward, inverse compensation, virtual coupling, Smith regulator, fuzzy logic, three variable control, infinite impulse response, impedance matching or adaptive compensation. A summary of the time-delay compensation methodologies studied for RTHS of structures is presented in Table 2.1.

Polynomial extrapolation

Horiuchi *et al.* [46] proposed the polynomial extrapolation method for a linear SDOF. The displacement of the actuator, $u(t)$, after the delay τ is obtained with the following expression:

$$u(t) = \sum_{i=0}^{n} a_i x_i \qquad (2.3)$$

where n is the order of the polynomial, $i = 0, 1, ..., n$, $x_i = x_m(t - i\tau)$ are the previously measured displacements at integer multiples of the time delay and a_i are the coefficients of the polynomial that are determined using the Lagrange basis functions. An example of this method is the fourth-order polynomial used by Darby *et al.* [55] that takes the following form:

$$u(t) = 5x_0 - 10x_1 + 10x_2 - 5x_3 + x_4 \qquad (2.4)$$

The experimental substructure becomes a SDOF dynamic system with an apparent stiffness (k^*) and damping (c^*) as a function of $\omega\tau$, where ω is the natural frequency of the structure. Therefore, structures with higher stiffness produce higher negative damping that could lead to unstable simulations. Horiuchi *et al.* [56] recommended third-order polynomial because it requires small calculations loads and gives large critical value of $\omega\tau = 1.571$. For simulations considering MDOF systems, the highest natural frequency must be used as the excitation frequency ω.

Darby *et al.* [57] use interpolation between two extrapolated points in order to have a smooth displacement variation between time-step samples to improve accuracy of SDOF RTHS with non-linear structures. Later, Horiuchi and Konno [58] proposed a linear extrapolation of acceleration measruement to improve stability.

Wu *et al.* [59] proposed an upper-bound delay compensation to obtain an optimal feedback displacement for nonlinear MDOF structures. This approach requires an initial overcompensation of displacement, which can be obtained with Hermite extrapolation, explicit Newmark, or linear acceleration extrapolation [58]. As an example, the second-order Hermit extrapolation is shown below:

$$u_k^* = (1 - \eta^2)x_{k+1} + \eta^2 x_k + (\eta + \eta^2)T_s \dot{x}_{k+1} \tag{2.5}$$

where u_k^* is the overcompensated displacement, x_{k+1} and x_k are predicted displacements, $\dot{x}_{k+1}$ is the predicted velocity, k is the time step index, T_s is the sampling time, τ_c is the upper bound delay estimated with the initial stiffness of the experimental substructure, and η is the time delay ratio τ_c/T_s. The overcompensated displacement is sent out as a command to the actuator and closest displacement $\mathbf{x}_m$ to u_k^* is used as the targed displacement. The corresponding measured force $\mathbf{f}_e$ is fed back to the numerical substructure as seen in Fig. 3.3.

Zhu *et al.* [60] proposed the Dual Explicit Prediction Methodology which is constructed by displacement extrapolation and the explicit numerical integration method Gui-λ proposed by Gui *et al.* [61]. The predicted displacement can be calculated by using the following expression:

$$u_k = x_{k+1} + \tau \dot{x}_{k+1} + \alpha_g \tau^2 \ddot{x}_{k+1}^* \tag{2.6}$$

where $\ddot{x}_{k+1}^*$ is the predicted acceleration, obtained from a fourth-order polynomial; x_{k+1}, $\dot{x}_{k+1}$ and α_g are extrapolated displacement, extrapolated velocity and an integration parameter, respectively, which are computed by:

$$x_{k+1} = x_k + T_s \dot{x}_k + \alpha_g T_s^2 \ddot{x}_k \tag{2.7}$$

$$\dot{x}_{k+1} = \dot{x}_k + \alpha_g T_s \ddot{x}_k \tag{2.8}$$

$$\alpha_g = 2\lambda(2\lambda \mathbf{M}_n + \lambda T_s \mathbf{C}_n + 2T_s^2 \mathbf{K}_n)^{-1} \mathbf{M}_n \tag{2.9}$$

where λ is the integration method parameter that is varied to guarantee stability and $\mathbf{M}_n, \mathbf{C}_n, \mathbf{K}_n$ are the mass, damping and stiffness matrices of the numerical substructure, respectively. This method is particularly useful for simulation with large time step integration.

15

Ning *et al.* [62] developed a robust compensation scheme based on polynomial extrapolation. The proposed controller is composed of three components: a mixed sensitivity-based robust H_∞ controller to stabilize the plant dynamics, an adaptive filter made of a Kalman filter and a model-based minimum mean square error estimator used to reduce the effect of measurement noise, and the polynomial extrapolation for time delay compensation that uses the following equation:

$$
\begin{aligned}
u_k = & \left(1 + \frac{11}{6}\eta + \eta^2 + \frac{1}{6}\eta^3\right) x_k - \left(3\eta + \frac{3}{2}\eta^2 + \frac{1}{2}\eta^3\right) x_{k-1} \\
& + \left(\frac{3}{2}\eta + 2\eta^2 + \frac{1}{2}\eta^3\right) x_{k-2} - \left(\frac{1}{3}\eta + \frac{1}{2}\eta^2 + \frac{1}{6}\eta^3\right) x_{k-3}
\end{aligned}
\tag{2.10}
$$

where x is the displacement obtained from the numerical substructure at different time steps k and $\eta = \tau/T_s$.

Recently, Zhou *et al.* [63] proposed a Robust Linear Quadratic Gaussian (RLQG) controller by combining polynomial feed-forward prediction, Linear Quadratic Gaussian (LQG) controller and a Loop Transfer Recovery (LTR) procedure. The robustness provided by LTR is evaluated with the vRTHS benchmark problem [43].

Phase-Lead Compensation

Zhao *et al.* [45] implemented the Phase-Lead Compensator (PLC) for RTHS to improve amplitude and phase errors. The transfer function is given by:

$$
G_c(s) = \frac{\tau s + 1}{\alpha_p \tau s + 1}
\tag{2.11}
$$

where α_p is the phase-lead constant and s is the frequency-domain variable. The maximum phase angle introduced is decided by α_p. In general, this approach can contribute a maximum of 60°. This method requires an accurate estimation of the time delay for its implementation because under-compensation affects accuracy and overcompensation might lead to instability.

Jung *et al.* [64] compared phase-lead compensation with feed-forward compensation and showed that the later was useful to correct displacement errors in the reaction frame.

Model-based Compensation

Carrion and Spencer [44] proposed the Model-based Compensation approach. It uses known information of the structure such as the mass matrix, damping matrix, the initial elastic stiffness of the structure, and the external excitation $(\ddot{x}_g)$. The transfer function of the experimental substructure is deduced from of a linearized model as follows:

$$G_p(s) = \frac{\kappa_m}{\prod_{i=1}^{n}(s - p_i)} \qquad (2.12)$$

where n is the order of the controller, κ_m is the gain and p_i are the poles. The dynamics of the servo-hydraulic system are cancelled with an inverse-based feed-forward controller. A unit-low pass filter is implemented to avoid an improper transfer function:

$$G_c(s) = \alpha_m^n \frac{\prod_{i=1}^{n}(s - p_i)}{\prod_{i=1}^{n}(s - \alpha_m p_i)} \qquad (2.13)$$

This formulation is useful for inelastic systems because it can introduce a proportional feedback (K_{fb}) to reduce model uncertainties. Phillips and Spencer [65] extended the idea where the improper inverse transfer function is a nth order polynomial in the Laplace domain and the discrete time controller for a three-pole model takes the following form:

$$u_k = a_0 x_k + a_1 \dot{x}_k + a_2 \ddot{x}_k + a_3 \dddot{x}_k \qquad (2.14)$$

The higher order derivatives should be obtained from the numerical integration to avoid noise propagation, they can also be obtained with the Central Difference Method (CDM). The proportional feedback controller was replaced with a LQG optimal control algorithm. Phillips *et al.* [66] adopted the backward-difference method to estimate the higher order derivative to provide a general framework for controller development. The main limitation of CDM is the lack of a framework to estimate derivatives beyond the fourth-order, which may be necessary for higher-order feed-forward controllers.

Nakata and Stehman [67] implemented model-based compensation for SDOF RTH-STT. The authors used a Kalman filter to estimate the states of the SDOF because the structural response used in the feedback process was not measured in the experimental process. Hayati and Song [68] used a discrete-time model-based feed-forward

control methodology for input with frequency bandwidth of 0-30 Hz. The authors adopted a Finite Impulse Response filter (FIR) designed based on autoregressive with exogenous input (ARX) model of the SDOF system.

Gao *et al.* [49] integrated an outer-loop digital H_∞ robust controller with the model-based approach. The controller has a unity-gain negative feedback form with an incorporated low-pass filter. The controller design is based on the trade-off between tracking performance and control robustness; however, this strategy introduces an artificial mode of vibration that may affect the performance of the simulation if the frequency content of the noise is close to the frequency of the artificial mode. Later, Ou *et al.* [69] implemented the Robust Integrated Actuator Control (RIAC) that is based on the H_∞ algorithm, the model-based compensation, and a linear-quadratic estimation algorithm (LQE). This approach showed a considerable reduction of noise effect compared to the controller proposed by Gao *et al.* [49], while maintaining the same stability characteristics.

Derivative feed-forward

Jung *et al.* [70] used the Derivative Feed-Forward compensation (DFC) to study non-linear structural systems. The command displacement is modified by the weighted error from previous time-step. The discrete-time tracking controller takes the following form:

$$G_c(z) = \frac{G_{PID}(z) + G_{ff}(z)}{G_{PID}(z)} \tag{2.15}$$

where $G_{PID}(z)$ is the digital proportional-integral-derivative (PID) servo-controller, $G_{ff}(z)$ is the discrete transfer function that calculates the derivative of the interpolated command displacements from the ramp generator and adds them to the displacement signal for the servo-hydraulic actuator, it is obtained as follows:

$$G_{ff}(z) = k_{ff} \frac{(z-1)}{T_s z} \tag{2.16}$$

where z is the discrete time variable and k_{ff} is the feed-forward gain.

Inverse Compensation

The hydraulic actuator used in RTHS at the coupling between substructures can be modeled as a first-order system [71]:

$$G_m(s) = \frac{b_m}{s + a_m} \tag{2.17}$$

where $G_m(s)$ is the transfer function of the actuator model, b_m is a low-frequency gain and a_m defines the cut-off frequency. Chen [72] used this approach and proposed a discrete-time inverse compensation scheme, where the transfer function is:

$$G_c(z) = \frac{\alpha z - (\alpha - 1)}{z} \tag{2.18}$$

where z is the discrete time variable and α is the delay constant defined as:

$$\alpha = T_s/\tau + 1 \tag{2.19}$$

This approach requires an accurate estimation of α before the test to guarantee stability. Chen and Ricles [73] refined this strategy with a dual compensation system to avoid the exact estimation of the actuator delay. The tracking error between the command displacement and measured displacement is multiplied by a proportional gain k and fed back to the system, the transfer function between command displacement and measured displacement is formulated as:

$$G(z) = \frac{\alpha_{es}(z - 1) + (1 + \gamma)}{\alpha_{ex}(z - 1) + (1 + \gamma)} \tag{2.20}$$

where α_{es} is the estimated delay constant, α_{ex} is the actual delay constant value and γ is a proportional gain. The value of the proportional gain γ is calibrated to obtain accurate results of RTHS.

Virtual Coupling

Christenson *et al.* [6] implemented a virtual coupling between the physical and numerical substructure to improve stability against time delay. The transfer function is expressed as follows:

$$G_c(s) = c_v s + k_v \tag{2.21}$$

where c_v and k_v are the damping and the stiffness of the virtual coupling, respectively. The proposed approach can be interpreted as a first-order feed-forward

controller. A virtual stiffness higher than the real stiffness improves accuracy and similar stiffness reduces time delay. The two parameters need to be calibrated because there is a trade-off between performance and stability, the balance between the two parameters is adjusted according the the stiffness of the physical substructure. When the restoring force $\mathbf{f}_e$ shown in Fig. 3.3 becomes significant relative to the virtual stiffness, the simulation has higher stability but reduces performance.

Smith-type Predictor

Shao and Reihorn [74] used a Smith-type predictor to reduce time delay in a SDOF forced based RTHSTT. The control method is used a series elasticity actuator with displacement feedback. It consists in placing an elastic spring between the actuator and the physical substructure and the actuator is controlled with a displacement feedback to obtain the necessary force output using the Hooke's Law. The time delay compensation is achieved with the Smith's predictor, the transfer function takes the following form:

$$G_c(s) = \frac{G_p(s)}{1 - G_p(s)} \mathbf{f}_e \tag{2.22}$$

where $G_p(s)$ is the estimated plant model. The authors state that the proposed platform can be applied for studying RTHS of MDOF structures.

Fuzzy Logic-based control methodology

Verma *et al.* [75] studied a Takagi-Sugeno-type control methodology based on fuzzy logic for RTHS of SDOF nonlinear systems where the output of the controller is given by:

$$u_k = \frac{\sum_{i=1}^{n} \sigma_i v_i}{\sum_{i=1}^{n} \sigma_i} \tag{2.23}$$

where u_k is the displacement command, n is the number of rules, $\sigma_i \in [0, 1]$ is the firing degree of the rule i, and v_i is the control output of the rule i.

The proposed controller is designed for two inputs and one output. The inputs are error e_k and rate of change in error $\dot{e}_k$ of the actuator displacement, and the output is the change in the control signal Δu_k. The control strategy maps the normalized input variables to the output signal based on five fuzzy sets: large negative (LN), small negative (SN), zero (ZE), small positive (SP) and large positive (LP). The obtained

change in the control signal is added to the past value of the control signal and then this value is denormalized to obtain the actual command displacement. The process of normalization and denormalization requires three gains that are determined using the Particle Swarm Optimization (PSO) algorithm, where the objective function is the minimization of the error e_k. This approach gives robustness to the simulation; however, it presents difficulties for structures with low damping ratios.

Three Variable Control

Günay and Mosalam [76] used a Three Variable Control (TVC) scheme to study the accuracy of accurate RTHSTT. The conventional TVC is a state variable feedback control with three kinematic variables: displacement, velocity, and acceleration. This approach is commonly used in shaking tables; however, for RTHSTT a modified TVC is proposed with four main components: reference generator, feedback generator, Delta-P stabilization and determination of servo-valve command.

The reference generator provides the command input, in this case only the displacement variable is considered and is later differentiated three times to obtain velocity, acceleration and jerk command. The feedback generator uses a cross-over filter to convert the measured displacement and acceleration into displacement, velocity and acceleration feedbacks to be used in the control process. The hydraulic fluid in the actuator and the shaking table behave as a SDOF system; therefore, the Delta-P stabilization is used to eliminates the response of this system. The last step to determine the servo-valve command is the use of the notch filters that attenuate the response in a specific frequency range. The proposed controller improved the acceleration response of RTHSTT and it was implemented to the HS system at the former NEES facility previously located at the University of California, Berkeley.

Infinite-Impulse-Response Compensation

Stehman and Nakata [77] proposed an Infinite-Impulse-Response (IIR) compensation technique for RTHSTT. The transfer function of the tracking controller takes the following form:

$$G_c(s) = [G_h(s)]^{-1} H_f(s) \tag{2.24}$$

where $H_f(s)$ is a low pass filter and $G_h(s)$ is the model of the displacement tracking transfer function, it is given by:

$$G_h(s) = \frac{\sum_{i=0}^{n} b_i s^i}{\sum_{j=0}^{m} a_j s^i} \quad with \; m > n \tag{2.25}$$

where b_i and a_j are constants that define the behavior of the experimental substructure, n is the order of the numerator and m is the order of the denominator. The tracking controller transfer function $G_c(s)$ is proper when the required number of poles of the low-pass filter is $r = m - n + 1$.

The proposed approach can be applied when the parameters of the transfer function are chosen such that the closed loop system does not amplify high-frequency vibration. This controller showed good accuracy for RTHS with complex control-structure-interaction (CSI), a common issue in RTHSTT.

Impedance matching control

Verma and Sivaselvan [78] applied the approach of impedance matching to design a controller for the benchmark problem [43]. This approach considers the transfer system as two input single output system, where the earthquake excitation and the force feedback are the inputs and target displacement is the output. The numerical integration scheme is replaced with a transfer function of the numerical substructure and the controller transfer function is obtained from an appropriate state-space model of the components of the system.

Adaptive compensation

Tracking control methodologies based on adaptive compensation were developed to improve robustness to RTHS. This is required because time delay might vary during the RTHS, caused by actuator dynamics and nonlinearities in the experimental substructure. Adaptive compensation methods studied in RTHS are: minimal control synthesis, polynomial extrapolation, phase-lead compensation, inverse compensation, time series, and model-based compensation.

Minimal Control Synthesis

Minimal Control Synthesis (MCS) is an adaptive model reference control strategy that does not require any *a priori* knowledge of the plant dynamics. The command

22

displacement is obtained with the feed-forward feedback controller:

$$u(t) = K_m(t)x(t) + K_r(t)r(t) \tag{2.26}$$

where $x(t)$ is the displacement, $r(t)$ is the tracking error, $K(t)$ and $K_r(t)$ are the adaptive feed-forward and feedback gain, respectively, obtained as:

$$K_m(t) = \alpha_m \int_0^t r(\tau)x(\tau)d\tau + \beta r(t)x(t) + K_m(0) \tag{2.27}$$

$$K_r(t) = \alpha_m \int_0^t r(\tau)x(\tau)d\tau + \beta r(t)x(t) + K_r(0) \tag{2.28}$$

where $K_m(0)$ and $K_r(0)$ are set to zero, α_m and β are adaptive weights.

Neild *et al.* [79] implemented MCS for a SDOF system and proposed a method to reduce the effects of deterioration for high-order numerical models. Also, Neild *et al.* [80] implemented this scheme for RTHSTT. Lim *et al.* [81] proposed an alternative of the MCS method by changing the demand based on the numerical model of the substructure (MCSmd). Lim *et al.* [82] extended previous work by experimental implementation for linear substructures.

Bonnet [71] adopted the MCSmd adaptive controller including a first-order inverse model of the hydraulic actuator. The authors proposed a multi-tasking strategy to deal with different time-steps required for numerical integration and the MCSmd outer-loop controller.

Adaptive Polynomial Extrapolation

Darby *et al.* [83] proposed an on-line time delay estimation and compensation. The target displacement is given by:

$$u_k = (\tau_k^2 + 2T_s^2 - 3T_s\tau_k)\frac{x_{k+2}}{2T_s^2} - (\tau_k^2 - 2T_s\tau_k)\frac{x_{k+1}}{T_s^2} + (\tau_k^2 - T_s\tau_k)\frac{x_k}{2T_s^2} \tag{2.29}$$

where u_k is the command signal, T_s is the time-step, x is the extrapolated displacement obtained from Eq. 2.3 for the time steps k, $k+1$ and $k+2$, and τ_k is the estimated time delay obtained with the following estimator:

$$\tau_k = \tau_{k-1} + C_p \tanh\left(C_v\frac{u_k - \dot{u}_k}{T_s}\right)(u_k - x_m) \tag{2.30}$$

23

where C_v and C_p are velocity and proportional gains, respectively, that need to be calibrated for stability, and x_m is the measured displacement.

Later, Ahmadizadeh *et al.* [84] proposed a different time delay estimator as follows:

$$\tau_k = \tau_{k-1} + 2\xi T_s \frac{u_k^{avg} - x_{mk}^{avg}}{x_{mk} - x_{m(k-2)}} \tag{2.31}$$

$$u_k^{avg} = \frac{u_k + u_{k-1} + u_{k-2}}{3} \tag{2.32}$$

$$x_{mk}^{avg} = \frac{x_{mk} + x_{m(k-1)} + x_{m(k-2)}}{3} \tag{2.33}$$

where ξ is a learning gain, which should be adjusted based of the expected amount of variation in the time delay. The author used this estimator with the polynomial extrapolation assuming linear variation for the acceleration [58].

Wallace *et al.* [85] proposed an adaptive forward predictor (AFP). It consists of polynomial extrapolation and the coefficients are fitted with least-square estimation with previous N steps. The controller displacement is obtained with the following expression:

$$u_k = k_a \sum_{i=0}^{n} a_i P^i \tag{2.34}$$

where k_a is used to remove amplitude error and increase accuracy, P is the magnitude of the forward predictor, and a_i are the variable coefficients obtained as:

$$\mathbf{B} = \mathbf{X}_p[(\mathbf{X}_m^\intercal \mathbf{X}_m)^{-1}\mathbf{X}_m] \tag{2.35}$$

where $\mathbf{B}$ is the vector with the variable coefficients, $\mathbf{X_p} = [1 \ PT_s...P^N T_s^N]$, $\mathbf{X}_m = [1 \ \mathbf{x_m}...\mathbf{x_m^N}]$, $\mathbf{x_m} = [x_{mk} \ x_{m(k-1)}...x_{m(k-n)}]^\intercal$, N is the order of the polynomial and n is the desired number of previous samples.

Tu *et al.* [86] improved the method with respect to settling performance and numerical conditions using a new direct compensation and singular value decomposition methods. The authors also showed that AFP is outperformed by linear dynamic based controller (i.e [49], [80]). Zhou *et al.* [87] combined the AFP algorithm with the Equivalent Force Control (EFC) [88], a method that replaces the numerical integration with a force-feedback control loop. The authors showed the accuracy and

stability of the controller for SDOF linear and nonlinear substructures such as a linear spring and a magneto-rheological damper. Xu *et al.* [89] evaluated the performance of the improved AFP (IAFP) combined with a Sliding Mode Controller (SMC) to improve accuracy and robustness of RTHS. The proposed method was tested with the vRTHS benchmark problem [43] and with a linear SDOF system test.

Recently, Wang *et al.* [90] proposed a a two stage compensation using the polynomial extrapolation shown in Eq. 2.10 and an three parameter adaptive error reduction using least squares method and evaluated its accuracy with the benchmark problem [43].

Adaptive Phase-Lead

Chen and Tsai [91] proposed a dual compensation strategy. It consists in a second-order PLC based on the inverse model principle and a restoring force compensator (RFC). The latter was adopted to reduce the amplitude errors obtained at high-frequencies generated by the PLC. The discrete-time transfer function can be expressed as follows:

$$G_c(z) = \frac{[W_1 + (W_1 + W_2 + 1)\epsilon]z^2 + [W_2 - (W_1 + W_2 + 1)\epsilon]z + 1}{W_1 z^2 + W_2 z + 1} \tag{2.36}$$

where W_1 and W_2 are weighted parameters that need to be established to get poles inside the unit circle, and ϵ is an integer greater than zero. This parameter is updated online using a gradient adaptive law during the simulation. Recently, Tao and Mercan [92] proposed an adaptive phase-lead compensator with the following transfer function:

$$G_c(s) = \frac{b_0 + b_1 s}{1 + s} \tag{2.37}$$

where b_0 and b_1 are the adaptive parameters obtained from frequency domain-based error indicators using a Hamming window on the measured displacement.

Adaptive Inverse Compensation

Chen and Ricles [93] proposed an adaptive inverse compensation where the adaptive law is based on actuator tracking indicator proposed by Mercan [94]. The transfer function is as follows:

$$G_c(z) = \frac{(\alpha_{es} + \Delta\alpha)z - (\alpha_{es} + \Delta\alpha - 1)}{z} \tag{2.38}$$

where α_{es} is the estimated actuator delay and $\Delta\alpha$ is the adaptive parameter formulated as:

$$\Delta\alpha(t) = k_p I_d(t) + k_i \int_0^t I_d(\tau)d\tau \tag{2.39}$$

where k_i and k_p are integrative and proportional gains, respectively, and I_d is the tracking indicator based on the enclosed area of the hysteresis in the synchronized subspace plot (i.e. u_k vs x_m).

Chen and Ricles [95] introduced a second evolutionary variable based on the actuator displacement amplitude error to improve accuracy because the previous adaptive law depends only on the phase component of the system. The transfer function takes the following form:

$$G_c(z) = \frac{(k_{est} + \Delta k)(\alpha_{es} + \Delta\alpha)z - (\alpha_{es} + \Delta\alpha - 1)}{z} \tag{2.40}$$

where k_{est} is the initial estimate of the proportional gain for the actuator response, usually taken as 1, and Δk is the adaptive amplitude variable obtained as:

$$\Delta\alpha(t) = k_p I_a(t) + k_i \int_0^t I_a(\tau)d\tau \tag{2.41}$$

where I_a is an amplitude indicator.

Xu *et al.* [96] proposed the Windowed Frequency Evaluation Index compensation (WFEI) that consists of the adaptive inverse compensation method combined with the frequency evaluation index (FEI) to improve accuracy during tests. The FEI is enabled with a moving window technique for online estimation of the time delay. The authors used the vRTHS benchmark problem [43] to evaluate the performance and robustness of the controller and demonstrated that the proposed method provide accurate results despite variations in the time delay estimation.

Adaptive Time Series

Chae *et al.* [9] developed the discrete adaptive time series (ATS) compensator that updates its coefficients at each time step using the least squares method. This approach obtains the compensated displacement with the expression:

$$u_k = \sum_{i=0}^{n} \alpha_{ik} \frac{d^i x_k}{dt^j} \tag{2.42}$$

where α_{ik} are the adaptive compensation parameters. The values of the parameters are identified using the least squares estimation with the previous q states of the measured displacement x_m as follows:

$$\mathbf{A} = (\mathbf{X}_m^\intercal \mathbf{X}_m)^{-1} \mathbf{X}_m^\intercal \mathbf{U}_c \tag{2.43}$$

where $\mathbf{A} = [\alpha_{0k} \; \alpha_{1k} \cdots \alpha_{nk}]^\intercal$, $\mathbf{X}_m = [\mathbf{x_m} \; \dot{\mathbf{x}}_\mathbf{m} \cdots \frac{d^n}{dt^n}(\mathbf{x_m})]$, $\mathbf{x_m} = [x_{m(k-1)} \; x_{m(k-2)}...x_{m(k-q)}]^\intercal$, and $\mathbf{U_c} = [x_k \; x_{k-2} \cdots x_{k-q}]^\intercal$.

This method does not require a calibration of parameters; however, an initial estimation is needed to avoid degradation due to noise measurements in the system. The authors, implemented a second-order ATS and studied the accuracy and robustness of the method. Afterwards, Chae *et al.* [97] developed two force control method using the ATS compensator and compliance springs that are accurate for RTHS of axially stiff test structures. These force control methods do not require the modeling of a test structure, an important advantage for non-linear structures. Palacio-Betancur and Gutierrez Soto [98] implemented a Conditional ATS (CATS) for the vRTHS benchmark problem [43]. The parameter estimation was executed only for target displacements above a threshold value to reduce undesired dynamics at low amplitudes. Also, a recursive least square algorithm was adopted in the parameter estimation to reduce computational efforts during the simulation.

Adaptive Model-based compensation

The model based compensation shown in section 2.5 considered a linearized model of the servo-hydraulic system. It was adopted to simplify the analysis of nonlinearities in RTHS; however, when these nonlinearities are significant this controller is not robust enough. Chen *et al.* [99] proposed an adaptive model-based approach, the parameters a_i of the feed-forward controller shown in Eq. 2.14 are modified online using a gradient adaptive control law with an instantaneous cost function. A third order feed-forward controller was implemented with LQG as feedback controller and CDM was used to estimate higher-order derivatives.

Backstepping Adaptive Control

Ouyang *et al.* [100] proposed a Backstepping Adaptive Control for RTHS with SDOF experimental substructure. A first-principle actuator dynamic model is implemented to take into account servo-atuator dynamics. The model considers the

servo-controller, the servo-valve dynamics, the servo-valve flow and actuator dynamics. This model is implemented with the Lyapunov stability analysis to develop the adaptive control law.

Sliding mode control

Maghareh *et al.* [101] developed the Self-tuning Robust Control System (SRCSys) based on two nonlinear control principles, robustness and adaptation. The first layer of the controller uses the SMC to take into account the nonlinear behavior of the plant, and the second layer consists in a bounded adaptation law of the parameters of the controller. The accuracy of the controller was evaluated with two RTHS with highly uncertain physical specimens.

Table 2.1: Summary of time delay compensation methodologies for RTHS of structures

Researcher	Year	Type	Description	DOF	Remarks	Ref.
Hourichi *et al.*	1996	Polynomial	General method of polynomial extrapolation	SDOF	Demonstration of negative damping and developed the nth order polynomial extrapolation method	[46]
Hourichi and Konno	1999	Polynomial	Optimal polynomial extrapolation	SDOF	Proposed third-order polynomial, it requires small calculation load and gives large critical value of $\omega\tau = 1.571$	[56]
Nakashima and Masoka	1999	Polynomial	Extrapolation and interpolation procedure based on Langrangean polynomial	MDOF	Developed RTHS system that is capable of studying up to 10 DOF	[102]
Darby *et al.*	2001	Polynomial	Improved polynomial extrapolation	SDOF	Interpolates between two extrapolated points using quadratic itnerpolation	[57]
Hourichi and Konno	2001	Polynomial	Linear acceleration extrapolation	MDOF	Validation through digital signal processor (DSP)	[58]
Darby *et al.*	2002	Adaptive	Online time delay estimation and compenation through polynomial extrapolation	SDOF	Aim to develop compensation for nonlinear structures	[83]
Zhao *et al.*	2003	Phase-lead	Amplitude and delay compensation	SDOF	Requires good estimation of time delay, undercompensation affects accuracy and overcompensation might lead to instability	[45]

Researcher	Year	Type	Description	DOF	Remarks	Ref.
Lim *et al.*	2004	Adaptive	Minimal controller synthesis modified demand (MC-Smd)	MDOF	Modified the demand of MCS based on the numerical model of the substructure.	[81]
Neild *et al.*	2005	Adaptive	Minimal controller synthesis (MCS)	SDOF	Applied MCS for RTHSTT	[80]
Neild *et al.*	2005	Adaptive	Minimal controller synthesis (MCS)	SDOF	Proposed a method to reduce deteriorating effect of numerical models with high modes of vibration	[79]
Wallace *et al.*	2005	Adaptive	Adaptive forward prediction (AFP)	MDOF'	Considered polynomial extrapolation with least-square polynomial fitting instead of Lagrange basis functions	[85]
Jung *et al.*	2006	Derivative feed-forward	Discrete feed-forward compensation	SDOF	Assumes that tracking error is similar to previous steps	[70]
Bonnet *et al.*	2007	Adaptive	MCSmd outer loop controller using a first-order actuator model	MDOF	Developed multi-tasking programming enviroment to deal with different time steps	[71]
Carrion *et al.*	2007	Model-based	Feed-forward model based and proportional feed-backwards	SDOF	Reduce the effect of model uncertainty by taking into account the model of the experimental system and proportional feedback	[44]
Jung *et al.*	2007	Phase-lead	Feed-forward and first-order phase-lead	MDOF	Maximum phase increase depending on alpha.	[64]

Researcher	Year	Type	Description	DOF	Remarks	Ref.
Lim *et al.*	2007	Adaptive	MCSmd outer loop controller using a first-order actuator model	SDOF	Extended previous work [81] by experimental implementation of linear substructures	[82]
Ahmadizadeh *et al.*	2008	Adaptive	Modified online time delay estimation and polynomial extrapolation	SDOF	Modified previous online estimation. It does not need *a priori* information about the experimental setup	[84]
Christenson *et al.*	2008	Virtual coupling	First-order feed-forward controller	MDOF	Requires parameter calibration because there is a tradeoff between performance and stability	[6]
Chen and Ricles	2009	Inverse	Improved discrete-time inverse compensation	SDOF	Adds a secondary compensation consisting of a proportional gain applied to actuator control error	[73]
Chen *et al.*	2009	Inverse	Discrete time inverse compensation using first-order model of actuator	SDOF	Developed numerical integration algorithm and implemented inverse compenstion	[103]
Chen and Ricles	2010	Adaptive	Discrete-time Inverse adaptive compensation	SDOF	Adaptive law based on actuator tracking error	[93]
Phillips and Spencer	2011	Model-based	Feed-forward model based and LQG feed-backwards	SDOF	Replaces proportional feedback for LQG	[65]
Chen *et al.*	2012	Adaptive	Improved inverse adaptive compensation	SDOF	Introduced adaptive gain because previous formulation of inverse compensation only acounted for phase lag in the system	[95]

Researcher	Year	Type	Description	DOF	Remarks	Ref.
Shao *et al.*	2012	Smith-predictor	Forced based RTHSTT	MDOF	Developed a controller platform to implement the proposed controller	[74]
Chae *et al.*	2013	Adaptive	Adaptime time series (ATS)	SDOF	Developed a discrete-time controller where the coefficients are updated every time-step using least-square method	[9]
Chen and Tsai	2013	Adaptive	Dual compensation using a second order phase-lead (PLC) and online restoring force (RFC)	SDOF	PLC is based on inverse model principle and RFC is based on equilibrium of the equation of motion considering the tracking error	[91]
Gao *et al.*	2013	Model-based	H_∞ loop shaping design for robustness	SDOF	Used H_∞ to guarantee accuracy, and provide robustness against uncertainties and external disturbances; however, it introduces artificial mode of vibration that may affect accuracy	[49]
Wu *et al.*	2013	Polynomial	Overcompensation and optimal feedback displacement	MDOF	The optimal displacement is obtained from previous measurements, if the system has a time-delay higher than the upper-limit, the latter is used for compensation	[59]
Nakata *et al.*	2014	Model-based	State observer and model based compensation	SDOF	Adopted model-based method but the structural response can not be measured, therefore a state observer using Kalman filter was used to estimate state variables.	[67]

Researcher	Year	Type	Description	DOF	Remarks	Ref.
Phillips et al.	2014	Model-based	Feed-forward model based and feed-backwards LQG	SDOF	Method based on the Taylor series and adopted backward-difference method to estimate higher-order derivatives	[66]
Tu et al.	2014	Adaptive	Adaptive forward prediction (AFP)	SDOF	Improved AFP with respect to the settling performance and numerical conditions	[86]
Verma et al.	2014	Fuzzy logic	Takagi-sugeno-type fuzzy logic controller	SDOF	The gains are determined using the particle swarm optimization (PSO). It presents difficulties for structures with low damping ratio	[75]
Zhu et al.	2014	Polynomial	Based on explicit numerical integration	SDOF	Useful for simulation for integration with large time step because reduces high-frequency response error	[60]
Chen et al.	2015	Adaptive	Adaptive model based with gradient adaptive law	SDOF	Uses 3rd order model based controller with LQG feedback and CDM to estimate higher order derivatives	[99]
Gunay et al.	2015	TVC	Three-variable-control for RTHSTT	SDOF	Implemented the TVC advanced control method to an existing HS system	[76]
Ou et al.	2015	Model-based	Robust integrated actuator control (RIAC)	SDOF	Robustness with feedback control based on H_∞ optimization, and noise reduction with LQE	[69]
Stehman and Nakata	2016	IIR	Feed-forward infinite-impulse-response (IIR)	SDOF	Proposed for substructures with significant inertial components (substantial floor mass, shake tables); however, it can be applied for any RTHS	[77]

Researcher	Year	Type	Description	DOF	Remarks	Ref.
Zhou *et al.*	2017	Adaptive	Adaptive forward prediction (AFP) combined with effective force control (EFC)	SDOF	Improves EFC implementing AFP algorithm. Evaluates stability in linear and nonlinear systems	[87]
Chae *et al.*	2018	Adaptive	Force control methods with ATS	SDOF	These force control methods do not require the modeling of the experimental substructure, an important advantage for non-linear systems	[97]
Hayati and Song	2018	Model-based	Finite-impulse-response (FIR) compensator based on discrete time autoregressive with exogenous input (ARX) model of the plant	SDOF	Discrete-time model based feed-forward taking into account CSI. Design for a bandwidth of 0-30 Hz	[68]
Ning *et al.*	2019	Polynomial	Polynomial extrapolation scheme combined with H_∞ control	SDOF	Combined three components: H_∞ suboptimal controller, an adaptive filter composed of a Kalman filter and an estimator to reconstruct actuator displacement, and a polynomial extrapolation scheme to reduce time delay	[62]
Ouyang *et al.*	2019	Adaptive	Backstepping Adaptive Control	SDOF	Included servo-actutor dynamcis considering a first-principle actuator model in order to develop the adaptive law of the controller	[100]

Researcher	Year	Type	Description	DOF	Remarks	Ref.
Palacio-Betancur and Gutierrez Soto	2019	Adaptive	Conditonal ATS compensation	SDOF	Proposed parameter estimation for displacements higher than a threshold value to avoid undesired dynamics at low amplitudes. Also, adopted a recursive least square algorithm to reduce computational efforts during simulation	[98]
Xu *et al.*	2019	Adaptive	Windowed Frequency Evaluation Index (WFEI)	SDOF	Integrated the Frequency Evaluation Index (FEI) with the adaptive inverse compensation method. The online estimation of the time delay is enabled through a moving window technique	[96]
Xu *et al.*	2019	Adaptive	Improved Adaptive forward prediction (IAFP) combined with sliding mode controller (SMC)	SDOF	Evaluated the performance of the controller with the vRTHS benchmark problem and with RTHS on a linear SDOF system	[89]
Tao and Mercan	2019	Adaptive	Two degree of freedom adaptive phase-lead compensator (APLC)	SDOF	Improve frequency domain-based error indicators using a hamming window with an overlapping length of 7/8th of the length of the window	[92]
Verma and Sivaselvan	2019	Impedance matching	Impedance matching controller with eartquake excitation and feedback force as inputs	SDOF	The transfer system guarantees physical and virtual substructures synchronization without implementing time-step integration schemes	[78]

Researcher	Year	Type	Description	DOF	Remarks	Ref.
Wang *et al.*	2019	Adpative	Polynomial extrapolation scheme combined with three-parameter error reduction	SDOF	Combined three components: polynomial extrapolation, adaptive three-variable error reduction, and adaptive filter composed of a Kalman filter and an estimator to reconstruct actuator displacement	[90]
Zhou *et al.*	2019	Polynomial	Robust Linear Quadratic Gaussian (RLQG) controller combined with polynomial feed-forward prediction	SDOF	The robustness of the controller is provided by a Loop Transfer Recovery (LTR) based on a modified sstate observer design procedure	[63]
Maghareh *et al.*	2020	Adaptive	Self-tuning Robust Control System (SRCSys) with robustness and adaptation layers	SDOF	The adaptive parameters of the controller are bounded to avoid unbounded estimates in the presence of uncertainties. The controller showed good accuracy for unknown time-varying nonlinear system including structural component failure during the RTHS.	[101]

36

3 Adaptive tracking controller

3.1   General

The implementation of tracking controllers in RTHS is important to guarantee accuracy and stability during testing as mention in the previous Chapter 2. A wide variety of control strategies have been implemented in RTHS and their details are given in section 2.5.

The key features for controllers suitable for RTHS are time delay compensation of the actuation system dynamics and robustness against plant variations and external disturbances. For this reason, a significant number of researchers have adopted adaptive controllers such as the polynomial extrapolation compensator [83], [84], adaptive forward prediction compensator [85], adaptive minimal controller synthesis algorithm [82], adaptive second-order phase lead compensator [104] and adaptive model-based tracking controller [99]. The gains used in the mentioned adaptive control algorithms need to be calibrated before the RTHS, therefore, to overcome this limitation Chae *et al.* [9] introduced an adaptive time series (ATS) compensator that updates its coefficients at each time step using the least squares method.

This research proposes a new adaptive tracking controller called Conditional Adaptive Time Series (CATS) controller. The proposed method is based on the principle of the ATS compensator and provides improvements in online parameter estimation and issues related to simulations with large noise-to-signal ratio. The performance of the proposed methodology is evaluated with a benchmark control problem of a three-story building that was introduced to develop effective and robust transfer system tracking controllers for RTHS [43]. Also, this chapter shows the design process and a sensitivity study of control parameters.

3.2   Benchmark setup

The benchmark problem consists in a vRTHS implemented using MATLAB and Simulink computer programming. The numerical and physical substructures are mod-

eled and the interface between them is an hydraulic actuator which will be referred as the transfer system. This system has inherent dynamics that will affect the accuracy and stability of the simulation and a control algorithm is required to compensate these effects. The characteristics of the reference structure, the vRTHS, implementation constraints and evaluation criteria will be explained in the following section.

Reference model

The physical structure was previously designed by Gao [105] for the development of robust framework for RTHS. It consists of a three-story, two-bay moment resisting steel frame with lumped masses at each level. The frame is made of steel A570 Grade 50, with columns S3x5.7 and built-up beams with 50x6 mm webs and 38x6mm flanges, the geometric characteristics are shown in Fig. 3.1(a). The finite element (FE) model of the structure shown in 3.1(b) has three horizontal DOF, obtained from a 30 DOF model with elastic behaviour assuming (1) negligible axial deformation; (2) rigid diaphragm; (3) lumped mass at the middle of each span; and (4) applying static condensation to the rotational DOF. Proportional damping is assumed with the same damping ratio for the three modes of vibration.
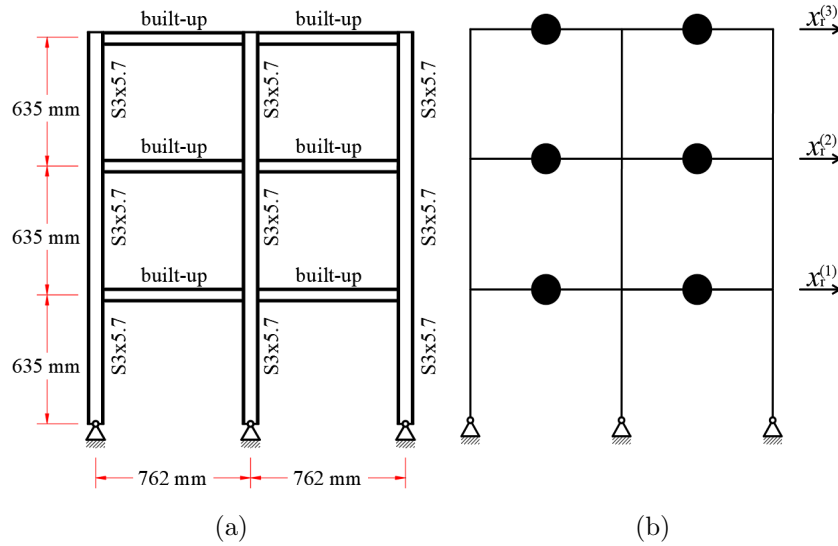

Figure 3.1: Reference Structure: (a) Physical Structure (b) Finite Element model

The equation of motion of the reference model shown in 3.1(b) is given by:

$$\mathbf{M_r}\ddot{\mathbf{x}} + \mathbf{C_r}\dot{\mathbf{x}} + \mathbf{K_r}\mathbf{x} = -\mathbf{M_r}\iota\ddot{x}_g \qquad (3.1)$$

38

where $\mathbf{M_r}, \mathbf{C_r}, \mathbf{K_r}$ are the mass, damping and stiffness matrix of the reference structure, respectively, $\mathbf{x}, \dot{\mathbf{x}}, \ddot{\mathbf{x}}$ are the displacement, velocity and acceleration vectors of the reference structure, respectively, relative to the ground, $\ddot{x}_g$ is the ground acceleration and ι is the influence coefficient vector.

Partitioning considerations

The partitioning of the reference structure into numerical and experimental substructures is shown in Fig. 3.2. The matrices of the system are:

$$
\begin{aligned}
\mathbf{M_r} &= \mathbf{M_e} + \mathbf{M_n} \\
\mathbf{C_r} &= \mathbf{C_e} + \mathbf{C_n} \\
\mathbf{K_r} &= \mathbf{K_e} + \mathbf{K_n}
\end{aligned}
\tag{3.2}
$$

where the subscripts e and n refer to experimental and numerical, respectively, and $\mathbf{M_e} = \mathrm{diag}(m_e, 0, 0)$, $\mathbf{C_e} = \mathrm{diag}(c_e, 0, 0)$ and $\mathbf{K_e} = \mathrm{diag}(k_e, 0, 0)$. The parameters m_e, c_e and k_e are the mass, damping and stiffness, respectively, of the experimental structure. Substituting Eqs. (3.2) into Eq. (3.1):

$$
\mathbf{M_n}\ddot{\mathbf{x}} + \mathbf{C_n}\dot{\mathbf{x}} + \mathbf{K_n}\mathbf{x} = -\mathbf{M_r}\iota\ddot{x}_g - \mathbf{f_e}
\tag{3.3}
$$

where $\mathbf{f_e} = \gamma f_e$ is the feedback force vector where γ is a column vector defined by spatial location of the interface DOF, in this case $\gamma = [1\ 0\ 0]^\intercal$, and f_e is the force at the first floor. The feedback force is obtained from the experimental substructure equivalent to $\mathbf{M_e}\ddot{\mathbf{x}} + \mathbf{C_e}\dot{\mathbf{x}} + \mathbf{K_e}\mathbf{x}$. Due to the dynamics of the actuator the force vector has an associated virtual time delay τ. The critical time delay τ_{cr} determines a stability switch where the simulation becomes unstable [48], it is a function of the partitioning choice. Additionally, a predictive stability indicator (PSI) formulated as PSI $= \log_{10}(\tau_{\mathrm{cr}})$ determines the sensitivity of a simulation to de-synchronization at the interface. The partitioning choices shown in Table 3.1 are considered for the design of the robust controller with PSI between 0.6 and 1.05, equivalent to time delays between 4 and 11 ms considered as moderately sensitive to slightly sensitive RTHS.

Control problem

The block diagram of the RTHS for the benchmark problem is shown in Fig. 3.3. The ground acceleration $(\ddot{x}_g)$ and the force feedback (f_e) are the input to the numerical
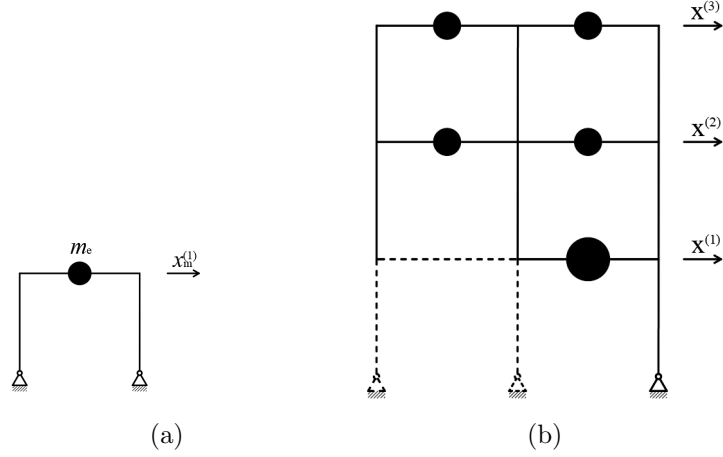
Figure 3.2: Reference structure partitioning: (a) experimental substructure and (b) numerical substructure

Table 3.1: RTHS partitioning cases of the benchmark problem

Case	Reference floor mass (kg)	Reference modal damping (%)
1	1000	5
2	1100	4
3	1300	3
4	1000	3

substructure, $\mathbf{y_n} = [\mathbf{x}\ \dot{\mathbf{x}}\ \ddot{\mathbf{x}}]^\intercal$ is the output that may be used as the input to the controller (G_C). The tracking controller generates the command signal y_{G_C} to the control plant (G_P) that consists in the transfer system and the experimental substructure. The sensors obtain the output vector y_{G_P} that contains the measured displacement and feedback force.
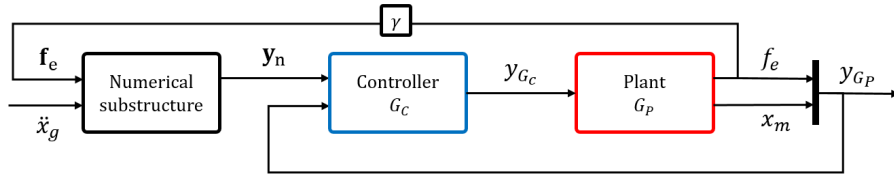
Figure 3.3: Block diagram of RTHS for the Benchmark problem

The numerical integration scheme adopted in the benchmark problem is an explicit fourth-order Runge-Kutta (ode4) with a fixed time step.

The model of the plant is obtained considering the servo-valve, hydraulic actuator, experimental substructure and control-structure interaction (CSI) [41]. This approach

was proposed by Magahareh *et al.* [42] in order to identify parameters for each component of the transfer system and experimental substructure. The plant closed loop response is given by

$$G_P(s) = \frac{B_0}{A_5 s^5 + A_4 s^4 + A_3 s^3 + A_2 s^2 + A_1 s + A_0} \tag{3.4}$$

where

$$
\begin{aligned}
B_0 &= a_1 \beta_0 \\
A_0 &= k_e a_3 \beta_2 + a_1 \beta_0 \\
A_1 &= k_e a_3 \beta_1 + (k_e + c_e a_3 + a_2) \beta_2 \\
A_2 &= k_e a_3 + (k_e + c_e a_3 + a_2) \beta_1 + (c_e + m_e a_3) \beta_2 \\
A_3 &= (k_e + c_e a_3 + a_2) + (c_e + m_e a_3) \beta_1 + m_e \beta_2 \\
A_4 &= c_e + m_e a_3 + m_e \beta_1 \\
A_5 &= m_e
\end{aligned}
\tag{3.5}
$$

The value of each parameter in Eq. 5 is shown in Table 3.2 which are obtained from the benchmark problem description [43].

Table 3.2: Parametric values of the plant from [43]

Parameter	Component	Nominal Value	Standard deviation	Units
$a_1 \beta_0$	Servo-valve	2.13×10^{13}	-	mPa/s
a_2	CSI	4.23×10^6	-	mPa
a_3	Actuator	3.3	1.3	1/s
β_1	Servo-valve	425	3.3	-
β_2	Servo-valve	10×10^4	3.3×10^3	1/s
m_e	Exp. mass	29.12	-	kg
k_e	Exp. stiff.	1.19×10^6	5×10^4	N/m
c_e	Exp. damp.	114.6	-	kg/s

The vRTHS benchmark problem is developed to enable researchers to model and test different tracking control methodologies in order to identify limitations and capabilities of each control strategy. The performance of the proposed adaptive actuator compensation methodology is evaluated in terms of robustness to noise and uncertainties in the modeling errors. These uncertainties are taken into account in perturbed models of the plant which is achieved by randomly generating parametric values from a normal distribution with the standard deviation shown in Table 3.2.

Simulation constraints

The vRTHS is subjected to the following constraints based on the physical devices available in the laboratory.

1. The controller has to be in discrete form.

2. The sampling frequency of the vRTHS is 4096 Hz.

3. The servo-hydraulic actuator response cannot exceed its maximum capacity of 8900 N, stroke of ± 7 mm and maximum velocity of ± 25 mm/s.

4. The A/D and D/A converters are with 18 bit precision and a span of ± 3.8 V, modeled as a saturation block and a quantizer in Simulink.

5. The sensor noise contains an RMS of 0.002 V modeled as a Gaussian rectangular pulse process with a width of 0.2 ms. The sensor conversion factors are 7.89 mm/V for displacement and 1096 N/V for force.

6. The controller can use as many states of $\mathbf{x_m}$, and elements of the output $\mathbf{y_n}$ and command $\mathbf{y_{G_P}}$ as needed.

7. The compensated time delay must be at least τ_{cr}.

8. The robustness must be evaluated with at least 20 perturbed models.

Evaluation criteria

To evaluate the performance of the controller, nine different evaluation criteria such as time delay, normalized root mean square (NRMS) and peak errorrs need to be obtained using the measured displacement ($\mathbf{x_m}$), the numerical substructure output ($\mathbf{y_n}$) and the reference structure response ($\mathbf{x_r}$). Each criterion with its equation is shown in Table 3.3.

3.3 Adaptive tracking control method

The tracking controller proposed for the benchmark problem consists in a proportional-integral-derivative (PID) feedback for the control plant (G_P) and a Conditional Adaptive Time Series (CATS) compensator for the command signal of the first floor $x_c^{(1)}$ as shown in Fig. 3.4. The design procedure and controller implementation is explained in the following subsections.

Table 3.3: Performance evaluation criteria

Criterion	Equation	Units
Time delay	$J_1 = \underset{k}{\text{argmax}} \left[\sum_1 y_n^{(1)}(i) x_m(i-k) \right]$	ms
Tracking error NRMS	$J_2 = \sqrt{\dfrac{\sum_{i=1}^{N}[x_m(i) - y_n^{(1)}(i)]^2}{\sum_{i=1}^{N}[y_n^{(1)}(i)]^2}} \times 100$	%
Peak tracking error	$J_3 = \dfrac{\max\left|x_m(i) - y_n^{(1)}(i)\right|}{\max\left|y_n^{(1)}(i)\right|} \times 100$	%
1st floor NRMS	$J_4 = \sqrt{\dfrac{\sum_{i=1}^{N}[x_m(i) - x_r^{(1)}(i)]^2}{\sum_{i=1}^{N}[x_r^{(1)}(i)]^2}} \times 100$	%
2nd floor NRMS	$J_5 = \sqrt{\dfrac{\sum_{i=1}^{N}[y_n^{(2)}(i) - x_r^{(2)}(i)]^2}{\sum_{i=1}^{N}[x_r^{(2)}(i)]^2}} \times 100$	%
3rd floor NRMS	$J_6 = \sqrt{\dfrac{\sum_{i=1}^{N}[y_n^{(3)}(i) - x_r^{(3)}(i)]^2}{\sum_{i=1}^{N}[x_r^{(3)}(i)]^2}} \times 100$	%
1st floor peak error	$J_7 = \dfrac{\max\left|x_m(i) - x_r^{(1)}(i)\right|}{\max\left|x_r^{(1)}(i)\right|} \times 100$	%
2nd floor peak error	$J_8 = \dfrac{\max\left|y_n^{(2)}(i) - x_r^{(2)}(i)\right|}{\max\left|x_r^{(2)}(i)\right|} \times 100$	%
3rd floor peak error	$J_9 = \dfrac{\max\left|y_n^{(3)}(i) - x_r^{(3)}(i)\right|}{\max\left|x_r^{(3)}(i)\right|} \times 100$	%

Feedback control

The PID controller is widely used for displacement control of servo-hydraulic actuator system, however, PID alone is not suitable for RTHS. For this reason, the adaptive actuator compensation architecture has additional components to mitigate time delay. The PID is designed for a percent overshoot less than 15%, rise time less than $0.01\,\text{s}$ and a maximum settling time of $0.1\,\text{s}$. The controller was designed based on the simulation of the plant subjected to a unit step in continuous-time and then the
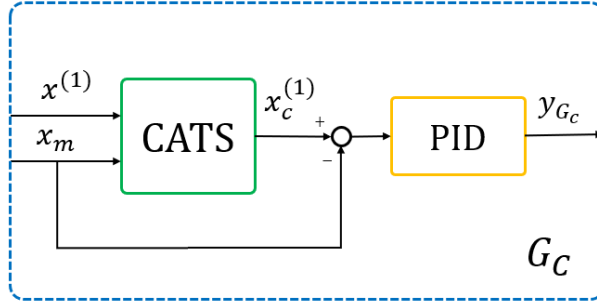
Figure 3.4: Tracking controller architecture

equation are converted to discrete time. The design objectives led to the gains $P = 1.8$, $I = 102$ and $D = 0$, and the unit step response of the system is shown in Fig. 3.5.
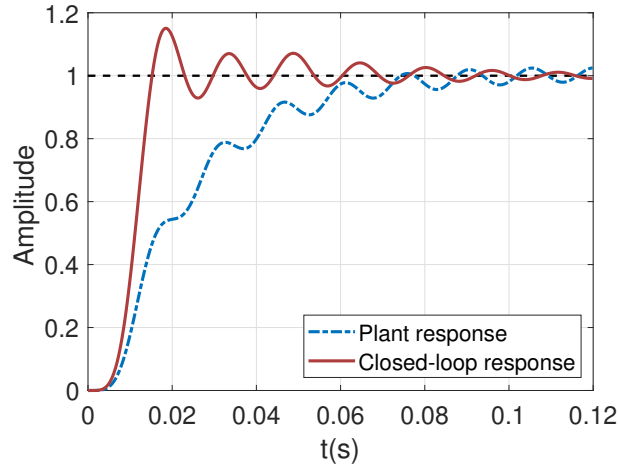
Figure 3.5: Unit step response comparison of the open-loop and closed-loop systems

The frequency response of the systems shown in Fig. 3.6 shows the improvement in amplitude using the PID control; however, it does not guarantee time delay compensation as mentioned previously.

Adaptive time series

The adaptive time series compensator (ATS) was proposed by Chae *et al.* [9]. The authors showed that the relationship between the command displacement $x_c^{(1)}$ and the input displacement $x^{(1)}$ of the plant with the PID feedback loop can be expressed

44
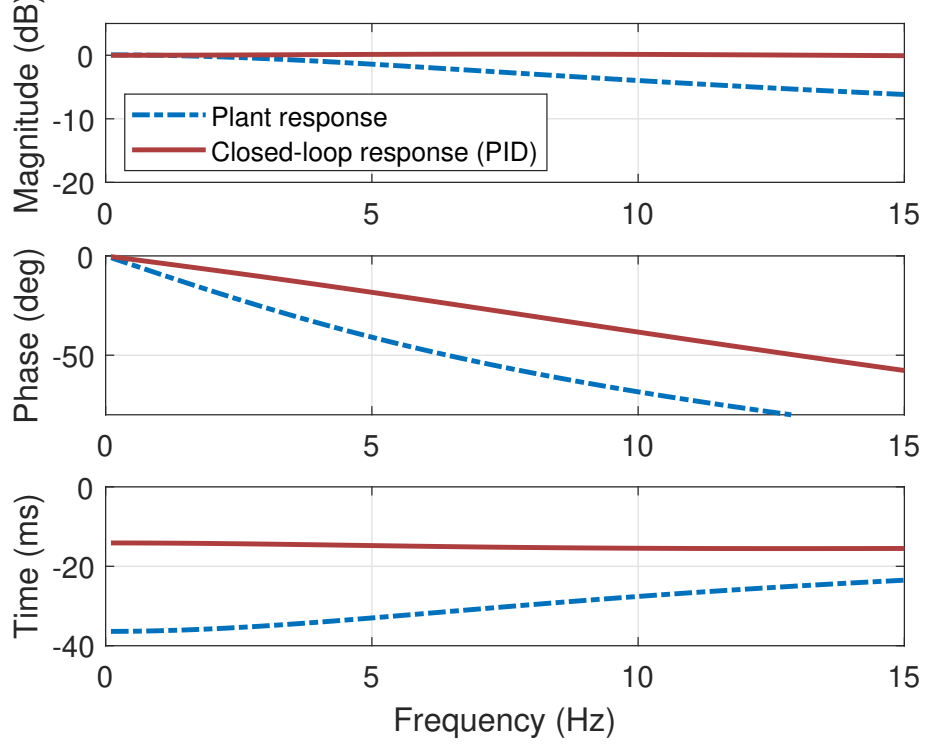
Figure 3.6: Frequency response comparison of the open-loop and closed-loop systems

as follows:

$$x_c^{(1)}(t) = \frac{1}{A} \sum_{j=0}^{n} \frac{\tau^j}{j!} \frac{d^j x^{(1)}(t)}{dt^j} \tag{3.6}$$

where A is the amplitude error, τ is the time delay of the system, ! is the factorial operator and n is the order of the compensator. Due to non-linearities of the plant, the actual amplitude error and time delay are not constant during the RTHS, therefore, an accurate actuator compensation is obtained using an estimate of the command displacement as shown in the following equation in discrete time:

$$x_c^{(1)}(k) = \sum_{j=0}^{n} \alpha_j \frac{d^j x^{(1)}(k)}{dt^j} \tag{3.7}$$

where k is the time step, $\alpha_{jk} = \tau^j / A_k j!$ for $j = 0, 1, ..., n$ are the adaptive compensation parameters, A_k is the amplitude error, τ_k is the time delay and $\frac{d^j x^{(1)}(k)}{dt^j}$ are time derivative obtained with finite difference method. The values of the compensation parameters can be identified using the least square estimation with a determined number of previous measured samples (x_m), more details about parameter estimation

45

will be explained in section 3.3. The amplitude error and the time delay can be obtain from the first two parameters as follows:

$$A_k = \frac{1}{\alpha_{0k}}, \ \tau_k = \frac{\alpha_{1k}}{\alpha_{0k}} \tag{3.8}$$

The accuracy of the simulation can be improved by using a high-order compensator, however, it may not be convenient because the higher order parameters can be affected by the noise in the force measurement [9]. Additionally, if a system has a low value of time delay, the influence of higher order terms may be negligible because α_{jk} decreases as a function of $j!$. Given that the PSI metric is related to the time delay, a relationship between the order of the required compensator and the PSI could be determined. A 1st and 2nd order ATS compensators were implemented and a similar performance was obtained. The 2nd order approach is not necessary because the variation of the third parameter (α_2) contributed between 0 and 1% of the total plant response. For example, in the benchmark problem, the maximum time delay is approximately 11 ms for the first partitioning case, using Eq.(3.8) and assuming an insignificant amplitude error ($A \approx 1$), the third parameter (α_2) would have a maximum magnitude of 6.05×10^{-5}. The reference structure is subjected to full scale of El Centro, Kobe and Morgan historical earthquakes that resulted on a maximum acceleration response in the first floor of $7.4\,\mathrm{m/s}$. Thus, the third parameter would compensate a maximum displacement of $0.05\,\mathrm{mm}$ which can be considered negligible for RTHS of maximum amplitude of $7\,\mathrm{mm}$ as stated in section 3.2. Therefore, only a first-order compensator will be implemented for the benchmark problem and the Simulink model for this approach is shown in Fig. 3.7.

To guarantee a good parameter estimation, the compensator requires a low-pass filter to remove the high frequency noise in the measured displacement, moreover, the same filter needs to be applied to the actuator command to synchronize the data for the parameter estimation. In this paper, a sixth-order Butterworth low-pass filter is used with a cut-off frequency of $6\,\mathrm{Hz}$ because the experimental substructure has a natural frequency between 3-4 Hz.

CATS initial parameters

The controller requires an estimation of initial values that reflect the behavior of the compensator, in this case a first-order approach. To obtain these values, the experimental substructure is subjected to a displacement command with a frequency
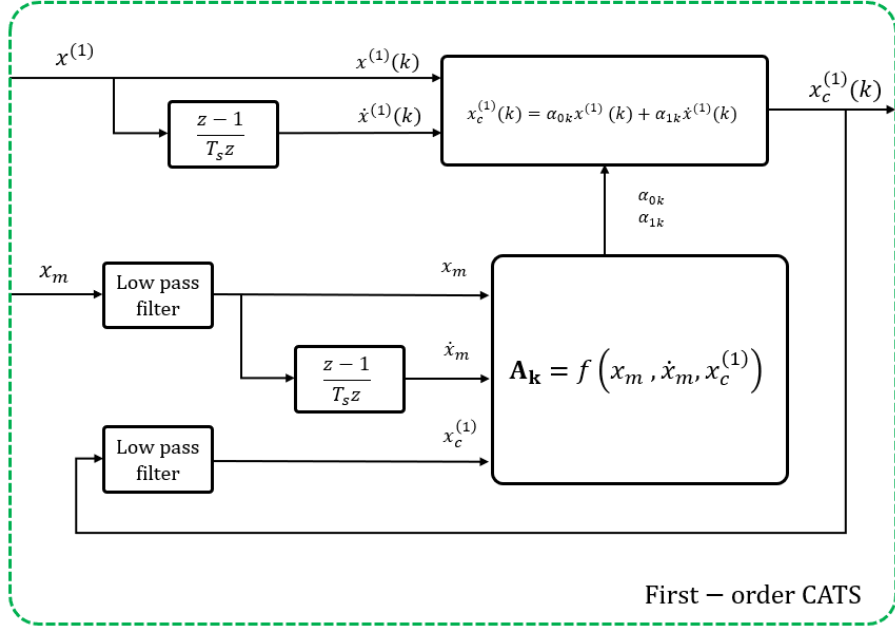
Figure 3.7: CATS Simulink model

content expected in the simulation. The model of the plant with the feedback controller, sensor and low-pass filter are subjected to a pre-defined displacement obtained from an artificial accelerogram generated by a well-known stationary stochastic process that uses a power spectral density proposed by Kanai [106] and Tajimi [107] and is formulated as:

$$S(\omega) = S_o \frac{\omega_g^4 + 4\zeta_z^2 + \omega_g^2\omega^2}{(\omega_g^2 - \omega^2)^2 + 4\zeta_z^2 + \omega_g^2\omega^2} \tag{3.9}$$

where ω_g is the ground frequency, ζ_g is the damping ratio and S_o is spectral intensity. The Kanai-Tajimi artificially generated accelerogram has been used in previous earthquake engineering studies [108]–[110]. Historical seismic events such as El Centro and Kobe can be represented using $\omega_g = 12, \zeta_g = 0.3$ and $\omega_g = 12, \zeta_g = 0.6$, respectively [111]. This paper uses ground frequency of $\omega_g = 9.4\,\text{rad/s}$, damping ratio of $\zeta = 0.34$, spectral intensity of $S_o = 1$ and the obtained accelerogram is scaled to obtain a maximum displacement of $5\,\text{mm}$. The input and measured displacements are shown in Fig. 3.8. Based on the least square method, using the data from 0 to $60.06\,\text{s}$ at a sampling frequency of $4096\,\text{Hz}$, the obtained initial parameters are $\alpha_0 = 0.9911$ and $\alpha_1 = 8.0542 \times 10^{-3}\text{s}$. Note that the second parameter is closely related to the time delay observed in the input-output relationship.

47
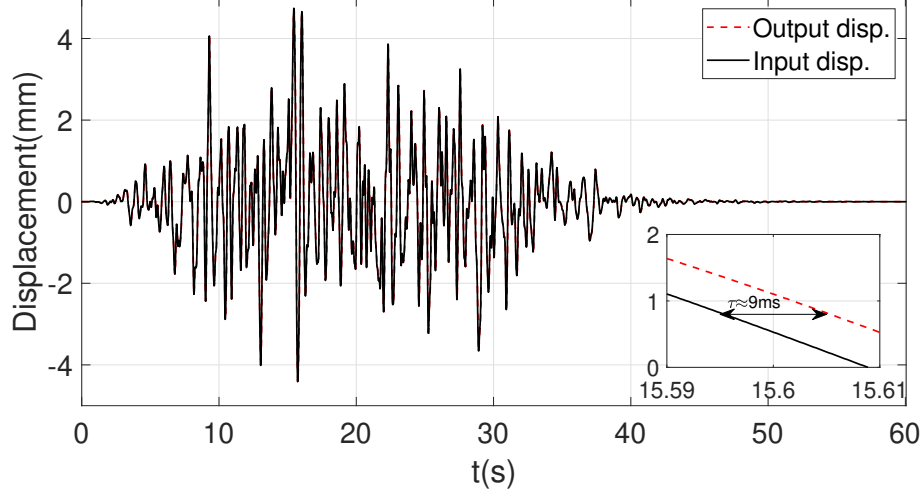
Figure 3.8: Displacement response of the plant subjected to Kanai-Tajimi artificially generated accelerogram (ω_g =9.4 rad/s, $\zeta = 0.34$, and $S_o = 1$)

To achieve a stable compensation, it is necessary to limit the range and rate of change of each parameter, these values are user-defined and their physical interpretation can be found in [9]. The chosen values are based on expected time delays and amplitude errors that are particular to the servo-hydraulic system and the experimental substructure, the values for the benchmark problem are shown in Table 3.4.

Table 3.4: CATS parameter limits

Parameter	Minimum	Maximum	Maximum rate $(\dfrac{\Delta a_{jk}}{T_s})$
α_0	0.8	1.2	2/s
α_1	0 s	0.02 s	0.05 s/s

Parameter estimation

A common approach for the parameter estimation is the least squares (LS) estimation. This method requires the use of previous states of the measured displacement x_m as follows:

$$\mathbf{A_k} = (\mathbf{X}_m^\intercal \mathbf{X}_m)^{-1} \mathbf{X}_m^\intercal \mathbf{U}_c \tag{3.10}$$

where $\mathbf{A_k} = [\alpha_{0k}\, \alpha_{1k} \cdots \alpha_{nk}]^\intercal$, $\mathbf{X}_m = [\mathbf{x_m}\ \dot{\mathbf{x}}_\mathbf{m} \cdots \frac{d^n}{dt^n}(\mathbf{x_m})]$, $\mathbf{x_m} = [x_{m(k-1)}\ x_{m(k-2)}...x_{m(k-q)}]^\intercal$, $\mathbf{U_c} = [x_{c(k-1)}^{(1)}\ x_{c(k-2)}^{(1)} \cdots x_{c(k-q)}^{(1)}]^\intercal$, and q is the number of previous steps used in the

parameter estimation. The accuracy of the estimation is affected by this sampling size. If it is small, the accuracy may not be assured. If it is large, it may compromise the simulation due to the required computational effort in the inversion of the matrices. A vRTHS is executed for different sampling sizes, which define a data window of $S_s = q/4096$ s, and the data is decimated by factors such that the vector $\mathbf{x}_m$ has length m. The NRMS of the tracking controller is obtained for each case when the first partitioned case is subjected to a 0.7 scaled El Centro historical earthquake and the results are shown in Table 3.5.

Table 3.5: NRMS (%) of sampling size test for 0.7 scaled El Centro historical earthquake

m $\diagdown$ S_s	0.5 s	1 s	1.5 s	2 s
32	1.53	1.44	1.42	1.40
64	1.53	1.45	1.43	1.40
128	1.53	1.45	1.43	1.41

Results show that accuracy is slightly improved for larger size of sampling and the decimation did not affect the results considerably. This means that the choice of sampling size and decimation factor for the benchmark problem is dependent on the computer speed where the RTHS is executed.

An alternative method for the parameter estimation is the recursive least square (RLS) algorithm. This approach eliminates redundant operations in the updating process because it only uses new information in each time step k and does not require previous measurements, making it faster than the commonly used LS algorithm. The adaptive parameters are obtained as follows:

$$\mathbf{A}_k = \mathbf{A}_{k-1} + \mathbf{\Phi} e_k \tag{3.11}$$

where $e_k = x_c^{(1)} - \mathbf{A}_k^\mathsf{T} \mathbf{X}_m$ is the error between command and measured signals, $\mathbf{X}_m = [x_m \ \dot{x}_m \cdots \frac{d^n}{dt^n}(x_m)]^\mathsf{T}$, and $\mathbf{\Phi}_k$ is known as the Kalman gain vector, which is formulated as:

$$\mathbf{\Phi}_k = \frac{\mathbf{P}_{k-1}\mathbf{X}_m}{\lambda + \mathbf{X}_m^\mathsf{T}\mathbf{P}_{k-1}\mathbf{X}_m} \tag{3.12}$$

where λ is the forgetting factor, which is problem dependent parameter and $\mathbf{P}_k$ is the inverse correlation matrix formulated as:

$$\mathbf{P}_k = \frac{\mathbf{P}_{k-1} - \mathbf{\Phi}_k \mathbf{X}_m^\intercal \mathbf{P}_{k-1}}{\lambda} \tag{3.13}$$

The initial conditions are set to $\mathbf{P}_o = \mathbf{I}_{nxn}$ and $\mathbf{A}_0$ as the vector with the initial parameters.

The selection between the shown algorithms depends on the characteristics of the computer where the RTHS is carried because both approaches yield similar results, for example the first partitioned case subjected to 0.35 scaled Kobe earthquake has a tracking error of 2.1% with LS and 2.26 % with RLS. A common practice is to implement LS algorithm with a sampling size of 1 s and the decimation factor can be chosen based on the capacity of the computer. On the other hand, the RLS algorithm is carried out faster and the forgetting factor λ is calibrated to obtain accurate results. The proposed CATS controller is implemented with the RLS algorithm for its low computational cost with $\mathbf{P}_o = \mathbf{I}_{2x2}$, $\mathbf{A}_0 = [\alpha_0 \; \alpha_1]$, and $\lambda = 0.998$.

Conditional adaptation

The accuracy at the beginning of the simulation, before the strong motion, may be affected by the measurement noise. A common practice with ATS controllers is to trigger the parameter estimation for a significant target displacement until the end of the simulation. In the benchmark problem it is reasonable to choose 0.1 mm given that the noise produces a maximum displacement error of 0.07 mm. A vRTHS is executed with the fourth partitioned case subjected to 0.35 scaled Kobe earthquake. The tracking error of 2.26% was obtained, however, the simulation has high-oscillation in regions with low amplitude as shown in Fig. 3.9(a).

Similar results were obtained with a vRTHS without noise, this means that the ATS controller introduces undesired dynamics to the system at low amplitudes, therefore, a new approach is proposed in this paper based on a conditional ATS. This new approach consists in executing parameter estimation **only** for target displacements above a threshold value, which is determined based on the characteristics of the system. For the benchmark problem the chosen threshold value is 1 mm. The vRTHS with the new approach, shown in Fig. 3.9(b), has better performance with a tracking error of 2.05% and eliminates the undesired high-oscillation.
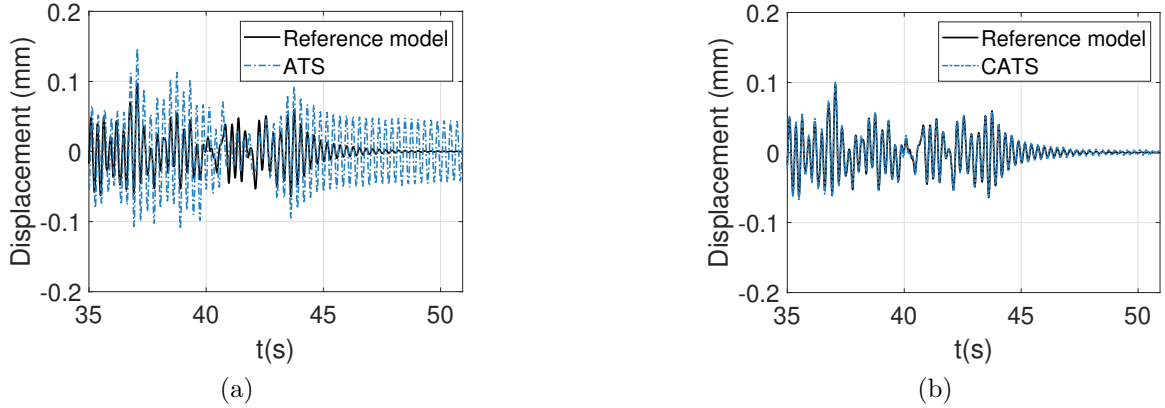
Figure 3.9: High-frequency oscillation at end of simulation when subjected to 0.35 scaled Kobe earthquake of Case 4 (a) ATS (b) CATS

Effect of measurement noise

The RTHS of low intensity earthquakes present a challenge that becomes important when the noise-to-signal ratio is large, which can be present when the capacity of the actuator is limited or measurement system is noisy. The measurement noise in the tracking control leads to an error propagation that degrades the performance of the simulation and generates a high frequency oscillation. This problem has been previously reported by other authors [69], [71] and the available solution to this problem is to increase the input earthquake intensity or improve hardware with small noise.

The CATS compensator has a low-pass filter that mitigates the effect of noise for parameter estimation, however, the feedback loop is still affected. A simulation is performed to examine the effects of the error propagation of small intensity earthquakes when the first partitioned case is subjected to a 0.2 scaled El Centro historical earthquake with different measurement noise levels with RMS of 0.002 V, 0.006 V, 0.01 V and 0.015 V.

The assessment of RTHS can be done from subspace plots where the target and measured displacement are compared, and a perfect simulation is represented by a 45° line. The results show the best performance for the lowest noise-to-signal ratio shown in Fig. 3.10(a), equivalent to the measurement noise in the benchmark problem. Higher levels of noise degrade performance as shown in the subspace plots in Fig. 3.10(b)-(d). The maximum time delay is only 0.2 ms, lower than the critical time delay (τ_{cr}) of the partitioned case, however, a decrease in performance is obtained. A
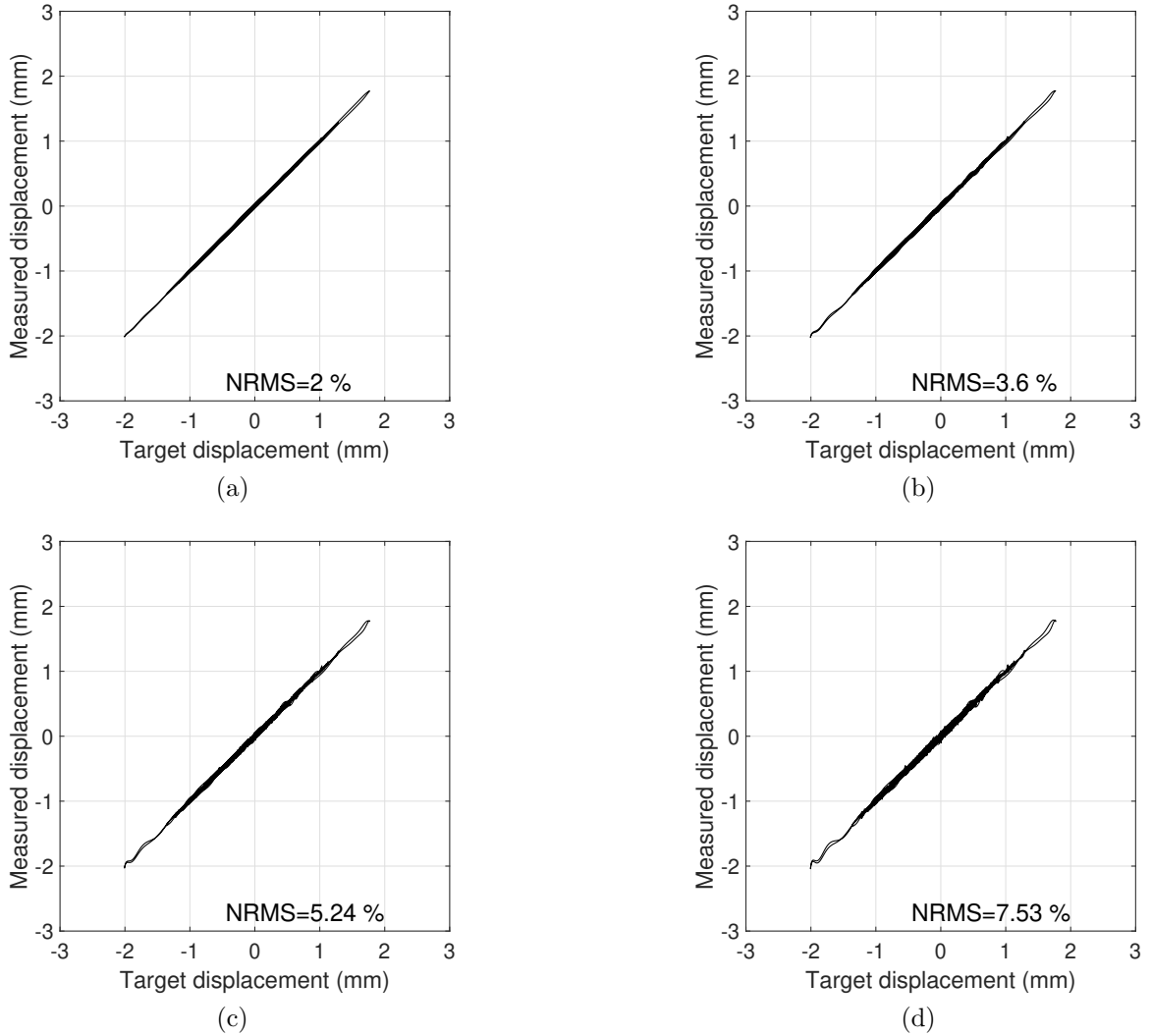
Figure 3.10: Effect of measurement noise (a) RMS $= 0.002\,\mathrm{V}$ (b)RMS $= 0.006\,\mathrm{V}$ (c) RMS $= 0.010\,\mathrm{V}$ (d) RMS $= 0.015\,\mathrm{V}$

similar degradation effect would occur if the analysis is done reducing the earthquake intensity for a fixed value of noise level because the noise-to-signal ratio increases. It is recommended to perform simulations with higher intensity and use a measurement system with the lowest noise possible.

3.4 Analysis and simulation

The vRTHS of the reference structure shown in Fig. 3.1 with the first partitioned case subjected to 0.35 scaled Kobe earthquake is implemented with three tracking controllers. The first one consist in the proposed first-order CATS controller, the

second is a first-order compensator without parameter adaptation (FO), and the last is the PID feedback controller with a phase-lead compensation (PL) proposed in the example implementation of the benchmark problem [43]. The benchmark feedback controller has the gains $P = 2$, $I = 95$ and $D = 0$, the gain of the phase-lead compensator is $k_T = 50.8$ and its zero-pole combination is $z_1 = -168.6$, $p_1 = -8570$. Fig. 3.11 shows the results of the first floor for both compensation approaches. The proposed tracking controller has better performance than the other two approaches, and Fig. 3.12 show the ability of the CATS parameters to take into account amplitude and time delay variation.
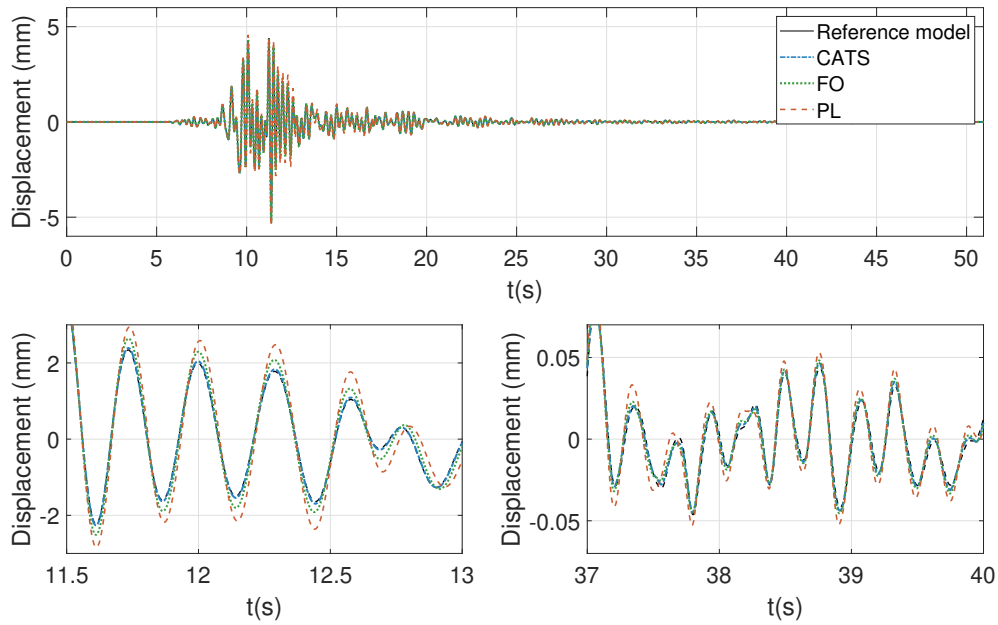
Figure 3.11: Comparison of the first floor displacement response between reference model, CATS compensator, FO compensator and PL compensator when subjected to 0.35 scaled Kobe earthquake of Case 1

Figure 3.13 show the results using the CATS compensator for partitioned cases 2-4 and the evaluation criteria of the used controllers is shown in Table 3.6. The first-order compensation, phase-lead compensation and the CATS compensation satisfy the simulation constraint of a time delay less than the critical time delay (τ_{cr}), however, the proposed approach has an improved accuracy and is capable of obtaining a time delay of $0\,$ms. Based on the comparison, it is clear that the CATS compensator provides better overall performance.

The robustness of the proposed controller is evaluated with a set of 5 perturbed

Figure 3.12: CATS compensation of 0.35 scaled Kobe earthquake Case 1 (a) Amplitude (b) Time delay

Table 3.6: Evaluation criteria comparison of Conditional Adaptive Time Series (CATS), First-Order (FO) and Phase Lead (PL) compensation schemes

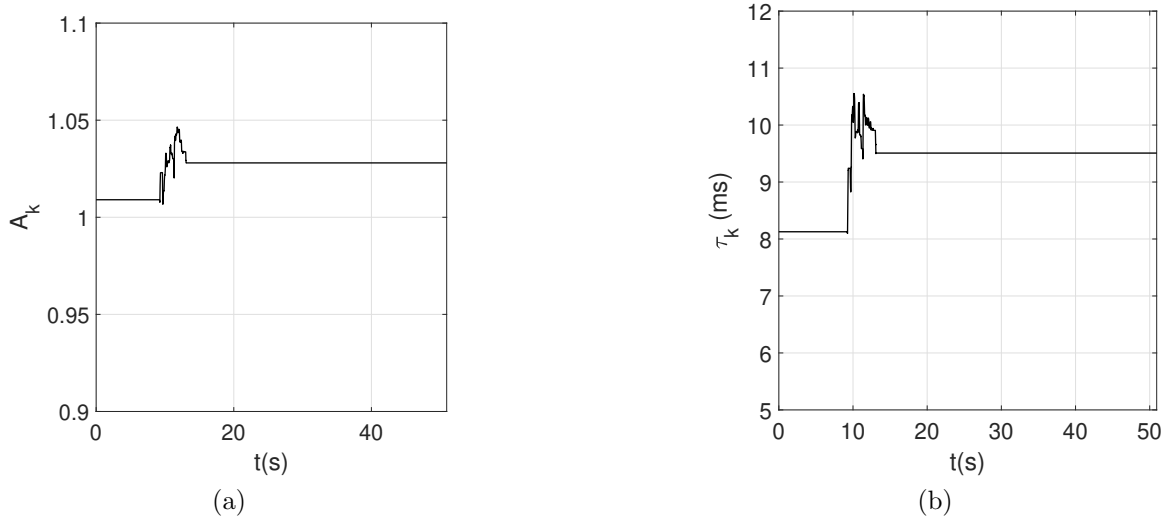| Case	Type	J_1	J_2	J_3	J_4	J_5	J_6	J_7	J_8	J_9
	CATS	0.2	2.3	2.2	3.8	**3.0**	**3.0**	3.1	2.1	2.1
1	FO	2.0	4.9	5.4	11.8	10.0	10.0	7.6	6.0	6.0
	PL	4.6	10.4	11.1	26.2	23.1	23.2	16.7	14.0	13.9
	CATS	**0.0**	2.1	2.4	3.9	3.2	3.2	3.2	2.3	2.2
2	FO	2.0	4.4	5.1	14.6	13.4	13.5	10.0	8.0	8.0
	PL	4.6	9.8	10.9	36.7	34.8	34.9	21.9	18.4	18.3
	CATS	**0.0**	**1.7**	**1.7**	**3.3**	**3.0**	**3.0**	**2.5**	**2.0**	**2.0**
3	FO	2.0	3.8	3.7	12.7	13.0	13.0	7.8	7.3	7.3
	PL	4.6	8.8	8.1	35.9	37.2	37.2	17.4	17.0	17.1
	CATS	0.2	2.1	2.3	4.9	4.3	4.3	3.6	2.7	2.7
4	FO	2.0	4.9	5.2	21.3	20.0	20.1	12.6	11.8	11.7
	PL	4.6	10.4	11.4	58.7	56.8	56.9	31.1	29.5	29.4

models for each partitioned case subjected to 0.35 scaled Kobe earthquake, this is achieved with random variations of the parameters of the nominal plant as explained in section 3.2. The average and maximum criteria for each partitioning case is shown in Table 3.7. The results indicate the ability of the controller to take into account changes in the plant reducing the time delay successfully closer to zero and guarantee accuracy for all the perturbed cases. The parameter $J1$ shows a maximum time delay of 0.2 ms, and the remaining evaluation criteria is below 6% for all partitioned cases.
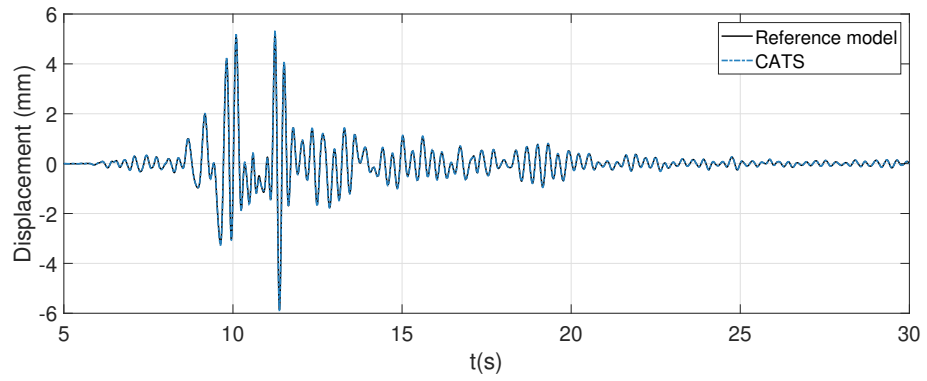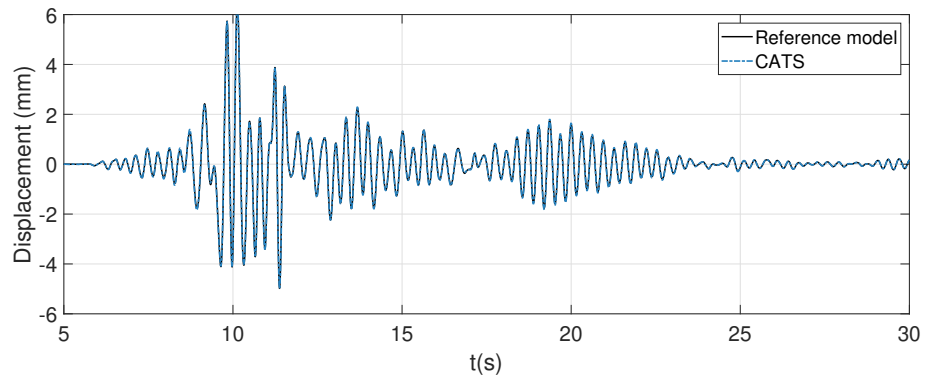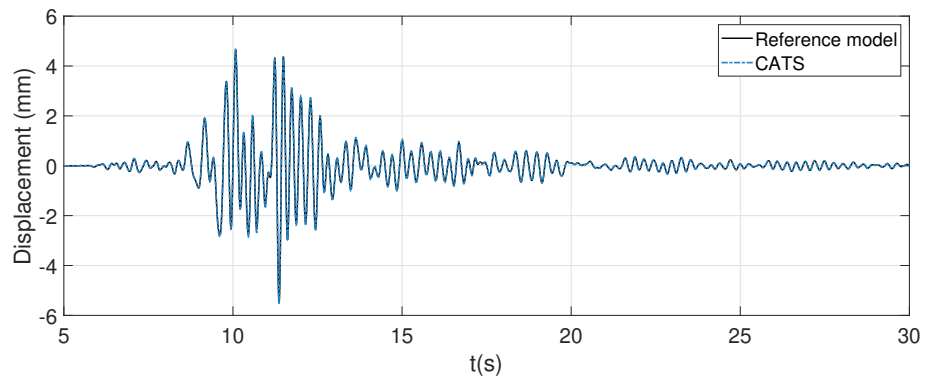
Figure 3.13: Displacement response of the first floor for (a) Case 2 (b) Case 3 (c) Case 4, when subjected to 0.35 scaled Kobe earthquake

Copyright© Alejandro Palacio-Betancur, 2020.

55

Table 3.7: Robustness assessment using CATS for 0.35 scaled Kobe earthquake

Case	Type	J_1	J_2	J_3	J_4	J_5	J_6	J_7	J_8	J_9
1	Avg.	0.2	2.29	2.18	3.86	3.04	3.05	3.17	2.10	2.11
	max	0.2	2.48	2.40	4.21	3.32	3.33	3.44	2.35	2.36
2	Avg.	**0.0**	2.18	2.40	3.95	3.23	3.23	3.30	2.30	2.27
	max	**0.0**	2.27	2.49	4.05	3.30	3.30	3.41	2.36	2.33
3	Avg.	**0.0**	**1.68**	**1.70**	**3.30**	**3.02**	**3.02**	**2.47**	**2.01**	**1.97**
	max	**0.0**	**2.04**	**2.15**	**3.63**	**3.23**	**3.22**	**2.84**	**2.23**	**2.18**
4	Avg.	0.2	2.05	2.30	4.97	4.40	4.41	3.59	2.75	2.72
	max	0.2	2.34	2.64	5.42	4.74	4.74	4.02	3.11	3.08

4 Numerical substructure

4.1   General

The previous chapters have focused on the development of tracking control algorithms to synchronize the the displacement between numerical and physical substructures. However, the numerical substructure modeling and dynamic response estimation also have an important role in the accuracy and stability of RTHS. Specially for the increased interest of enlargement of simulation scale. The time-step integration algorithms can be categorized into explicit and implicit. Explicit integration obtains the response only with information from previous steps which allows easy implementation and low computational cost. However, these methods are conditionally stable which limit the maximum time step of the RTHS. Implicit algorithms obtain the response based on current and previous steps, they are unconditionally stable but require higher computational cost compared to explicit methods. Bonnet *et al.* [112] compares six commonly used methods for RTHS in terms of accuracy, stability, computational cost, ease of implementation and suitability for non-linear analysis including the Newmark explicit, Newmark explicit unconditionally stable, the operator splitting method, the α-shifted operator splitting method, the constant average acceleration method and the Newmark implicit α-method. Wang *et al.* [113] compare the computational efficiency and accuracy of four explicit integration algorithms, the central difference method (CDM), the Newmark explicit method, the Chang method, and the Gui-λ method.

This study shows a comparative study of seven explicit numerical integration methods suitable for RTHS with the vRTHS benchmark problem shown in section 3.2 using the designed CATS controller of section 3.3.

4.2   Explicit numerical integration methods

This study considers seven commonly used integration algorithms for RTHS. The CDM is one of the most used algorithms due to its simple implementation [58]. Two Newmark methods can be unconditionally stable, the Newmark explicit scheme [112],

Newmark-Chang explicit [114] are implemented because they have been shown to be computationally efficient. Chen and Ricles [115] developed the CR algorithm using a discrete transfer function and pole mapping, it is unconditionally stable for RTHS. Kolay and Ricles [116] proposed the KR-α, an explicit unconditionally stable algorithm that introduces a parameter for numerical energy dissipation, a property useful for substructures with a large number of DOF. The fourth-order Runge-Kutta method is implemented for its simplicity and versatility in Simulink models [43]. Tang and Lou [117] developed the real-time substructure testing (RTS) method for SDOF, it is based using a discrete transfer function and applying mapping rule of poles. The calculation formulas of some of these methods are shown in Appendix A.

4.3 Analysis results

The vRTHS of the reference structure shwon in Fig. 3.1 with the fourth partitioned case subjected to 0.5 scaled El Centro earthquake is implemented for the seven explicit integration methods mentioned in the previous section. Fig. 4.1 shows the results of the first floor using the proposed CATS controller. From the details in Fig. 4.1 it is clear that the accuracy of the RTHS varies for each integration scheme because there are differences at low and high amplitudes.
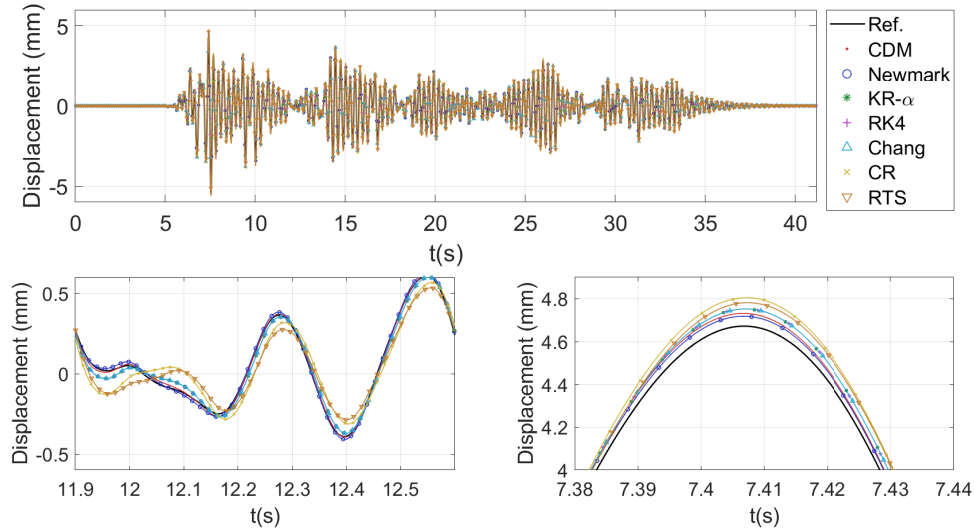

Figure 4.1: Accuracy assessment of numerical integration methods using CATS for 0.5 scaled El Centro earthquake

The evaluation criteria from Table 3.3 for each integration method is shown in Table 4.1. First, it is important to mention that the CATS controller yields the same

time delay (J_1) because this criteria is independent from the numerical substructure response. Then, the best agreement between the reference structure and the vRTHS was obtained with CDM and Newmark methods. The dissipative properties of KR-α method are useful in structures with high-number of DOF; therefore, no relevant differences were found for the benchmark problem.

Table 4.1: Accuracy assessment of numerical integration methods using CATS for 0.5 scaled El Centro earthquake

Method	J_1	J_2	J_3	J_4	J_5	J_6	J_7	J_8	J_9
CDM	0.2	1.35	**1.52**	2.10	1.56	1.57	2.57	1.79	1.78
Newmark	0.2	1.35	1.54	**1.77**	**1.27**	**1.26**	**2.43**	**1.6**	**1.59**
KR-α	0.2	1.34	1.56	3.71	3.26	3.27	2.92	2.11	2.11
RK4	0.2	**1.33**	1.56	3.70	3.25	3.26	2.92	2.11	2.11
Chang	0.2	1.34	1.56	3.71	3.25	3.27	2.91	2.11	2.12
CR	0.2	**1.33**	1.59	8.46	8.13	8.14	5.10	4.03	4.01
RTS	0.2	1.34	1.61	8.57	8.21	8.23	5.25	4.13	4.12

5 Conclusions and Recommendations for Further Research

5.1   Summary of Conclusions

This research presented a state of the art review of recent developments in tracking control methodologies to improve accuracy and robustness in RTHS of building structures subjected to natural hazards with a focus on seismic loading. A summary of the papers reviewed is presented in Table 2.1. The inherent dynamics of the actuators implemented for testing and the interaction between physical and experimental substructures lead to time delays that degrade the performance of the RTHS and jeopardize the stability of the system. The majority of studied compensation schemes are based on constant time delay; however, due to structural nonlinearities and actuator dynamics, innovative algorithms have been developed to address such challenges. This has generated an increased interest in adaptive compensation control methodologies that use error-based adaptation to account for changes in the overall system.

This study proposes a novel Conditional Adaptive Time Series (CATS) controller that consists in a PID feedback controller, a time series delay compensation, a conditional rule for parameter estimation, and a recursive least square (RLS) algorithm to reduce computational costs during simulation. The proposed method was designed for the benchmark problem consisting of a three story shear frame with one DOF in a vRTHS that considers numerical and experimental models subjected to earthquake loading. The stability of the controller is achieved by analysing the step response of the closed-loop system, identifying the range and maximum rate of change of the adaptive parameters, and by choosing a first-order compensator to improve the robustness to noise. The performance of the controller is evaluated with nine criteria for partitioned cases with different PSI values when the structures is subjected to historical earthquake loading. In addition, the performance was compared with a simple first-order compensator and the phase lead compensator proposed in the benchmark problem. Results show an overall good performance for the proposed controller for all partitioned cases where the system time delay was completely compensated and

the accuracy of the simulation has small errors.

Another important issue in RTHS is the presence of disturbances and noise in the feedback loop of the system. The noise-to-signal ratio plays an important part in the performance of a control methodology, when this ratio is high it causes a high-frequency oscillation in RTHS leading to an undesired performance degradation. The proposed controller presents challenges when the noise-to-signal ratio increases significantly which causes inaccurate tracking displacement, yet this limitation can be overcome by increasing the intensity of the earthquake if the physical system has enough capacity, and by implementing measurement systems with low noise. Some researchers implement state observers or adaptive filters to reduce the effect of noise. The robustness of the controller was evaluated for 20 perturbed models and it has the capability to adapt to this changes and obtain accurate results.

A comparative study of explicit integration methods was executed for one of the partitioned cases of the benchmark problem. These methods are efficient for RTHS for their explicit nature. Some of them require higher computational cost but they showed good overall performance using the CATS controller. The best agreement with the reference structure was obtained with CDM and Newmark and similar results were obtained with KR-a, RK4 and Chang methods. Note that the dissipative properties of KR-a method is useful in structures with high-number of DOF, in the benchmark problem no relevant different were found for different values of the dissipative parameter.

5.2   Recommendations for Further Research

Recent developments on RTHS have been focused on aspects of computation and communication speed, numerical integration methods, stability assessment tools, control design, and actuator compensation. These advances enable the study of smart structure technologies and other Civil Engineering applications due to the versatility and cost efficiency of the testing method. Nevertheless, there is an increased interest in enlargement of simulation scale and applications in highly nonlinear systems. Therefore, future research and implementation of this method include the design of accurate nonlinear controllers, the reduction of high noise-to-signal ratio inaccuracies, and computationally efficient numerical integration methods.

In addition, RTHS has the potential to enhance the current understanding of complex and large civil structures under multi-hazard scenarios. Several studies are focused on RTHS of structures subjected to earthquake loading and limited research was found using RTHS of structures subjected to other environmental or man-made hazards, such as windstorm events, tornado, tsunami loading, or blast loading.

A Explicit numerical integration methods

The equation 3.3 shown in section 3.2 can be rewritten as follows:

$$\mathbf{M_n}\ddot{\mathbf{x}}_k + \mathbf{C_n}\dot{\mathbf{x}}_k + \mathbf{K_n}\mathbf{x}_k = \mathbf{F}_{\mathbf{e}k} \tag{A.1}$$

where $\mathbf{x}_k, \dot{\mathbf{x}}_k, \ddot{\mathbf{x}}_k$ are the displacement, velocity and acceleration vectors of the reference structure at time step k, respectively, and $\mathbf{F_e}$ is the excitation vector of the numerical substructure obtained as:

$$\mathbf{F}_{\mathbf{e}k} = -\mathbf{M_r}\iota\ddot{x}_g - \mathbf{f_e} \tag{A.2}$$

Taking Δt as the time step, the basic formulas for each approach are shown below

A.1   CDM

$$\mathbf{x}_k = \frac{\mathbf{F}_{\mathbf{e}k-1} - \left(\mathbf{K_n} - 2\dfrac{\mathbf{M_n}}{\Delta t^2}\right)\mathbf{x}_{k-1} - \left(\dfrac{\mathbf{M_n}}{\Delta t^2} - \dfrac{\mathbf{C_n}}{2\Delta t}\right)\mathbf{x}_{k-2}}{\dfrac{\mathbf{M_n}}{\Delta t^2} + \dfrac{\mathbf{C_n}}{2\Delta t}} \tag{A.3}$$

A.2   Newmark

$$\mathbf{x}_k = \mathbf{x}_{k-1} + \Delta t\dot{\mathbf{x}}_{k-1} + \frac{1}{2}\Delta t^2\ddot{\mathbf{x}}_{k-1} \tag{A.4}$$

$$\dot{\mathbf{x}}_k = \dot{\mathbf{x}}_{k-1} + \frac{\Delta t}{2}(\ddot{\mathbf{x}}_k + \ddot{\mathbf{x}}_{k-1}) \tag{A.5}$$

$$\ddot{\mathbf{x}}_k = \frac{\mathbf{F}_{\mathbf{e}k} - \left(\dfrac{\mathbf{C_n}\Delta t}{2} + \dfrac{\mathbf{K_n}\Delta t^2}{2}\right)\ddot{\mathbf{x}}_{k-1} - (\mathbf{C_n} + \mathbf{K_n}\Delta t)\dot{\mathbf{x}}_{k-1} - \mathbf{K_n}\mathbf{x}_{k-1}}{\mathbf{M_n} + \dfrac{1}{2}\Delta t\mathbf{C_n}} \tag{A.6}$$

A.3 Chang

$$\beta_1 = \left(\mathbf{I} + \frac{1}{2}\Delta t \mathbf{M_n}^{-1}\mathbf{C_n} + \frac{1}{4}\Delta t^2 \mathbf{M_n}^{-1}\mathbf{K_n}\right)^{-1}\left(\mathbf{I} + \frac{1}{2}\Delta t \mathbf{M_n}^{-1}\mathbf{C_n}\right) \tag{A.7}$$

$$\beta_2 = \frac{1}{2}\left(\mathbf{I} + \frac{1}{2}\Delta t \mathbf{M_n}^{-1}\mathbf{C_n} + \frac{1}{4}\Delta t^2 \mathbf{M_n}^{-1}\mathbf{K_n}\right) \tag{A.8}$$

$$\mathbf{x}_k = \mathbf{x}_{k-1} + \beta_1 \Delta t \dot{\mathbf{x}}_{k-1} + \beta_2 \Delta t^2 \ddot{\mathbf{x}}_{k-1} \tag{A.9}$$

$$\dot{\mathbf{x}}_k = \dot{\mathbf{x}}_{k-1} + \frac{\Delta t}{2}(\ddot{\mathbf{x}}_k + \ddot{\mathbf{x}}_{k-1}) \tag{A.10}$$

$$\ddot{\mathbf{x}}_k = \frac{\mathbf{F}_{\mathbf{e}k} - \left(\dfrac{\mathbf{C_n}\Delta t}{2} + \beta_2 \mathbf{K_n}\Delta t^2\right)\ddot{\mathbf{x}}_{k-1} - \left(\mathbf{C_n} + \mathbf{K_n}\beta_1\Delta t\right)\dot{\mathbf{x}}_{k-1} - \mathbf{K_n}\mathbf{x}_{k-1}}{\mathbf{M_n} + \dfrac{1}{2}\Delta t \mathbf{C_n}} \tag{A.11}$$

A.4 CR

$$\alpha_{\mathbf{cr}} = \left(4\mathbf{M_n} + 4\mathbf{C_n}\Delta t + \mathbf{K_n}\Delta t^2\right)^{-1} 4\mathbf{M_n} \tag{A.12}$$

$$\ddot{\mathbf{x}}_k = \mathbf{M_n}^{-1}\left(\mathbf{F}_{\mathbf{e}k} - \mathbf{C_n}\dot{\mathbf{x}}_{k-1} - \mathbf{K_n}\ddot{\mathbf{x}}_{k-1}\right) \tag{A.13}$$

$$\dot{\mathbf{x}}_k = \dot{\mathbf{x}}_{k-1} + \alpha_{\mathbf{cr}}\Delta t \ddot{\mathbf{x}}_{k-1} \tag{A.14}$$

$$\mathbf{x}_k = \mathbf{x}_{k-1} + \Delta t \dot{\mathbf{x}}_{k-1} + \alpha_{\mathbf{cr}}\Delta t^2 \ddot{\mathbf{x}}_{k-1} \tag{A.15}$$

A.5 RTS

$$\mathbf{B_r} = 4\mathbf{M_n} + 2\Delta t \mathbf{C_n} + \Delta t^2 \mathbf{K_n} \tag{A.16}$$

$$\alpha_{\mathbf{r}} = 4\mathbf{B_r}^{-1}\mathbf{M_n} \tag{A.17}$$

$$\beta_{\mathbf{r}} = \mathbf{B_r}^{-1}\left(-2\left(\mathbf{M_n}^{-1}\mathbf{C_n}\mathbf{K_n}^{-1}\mathbf{M_n}\right)^2 - \Delta t \mathbf{C_n} + 4\mathbf{M_n}\right) \tag{A.18}$$

$$\ddot{\mathbf{x}}_k = \mathbf{M_n}^{-1}\left(\mathbf{F}_{\mathbf{e}k} - \mathbf{C_n}\dot{\mathbf{x}}_{k-1} - \mathbf{K_n}\ddot{\mathbf{x}}_{k-1}\right) \tag{A.19}$$

$$\dot{\mathbf{x}}_k = \dot{\mathbf{x}}_{k-1} + \alpha_{\mathbf{c}}\Delta t \ddot{\mathbf{x}}_{k-1} \tag{A.20}$$

$$\mathbf{x}_k = \mathbf{x}_{k-1} + \Delta t \dot{\mathbf{x}}_{k-1} + \beta_{\mathbf{r}}\Delta t^2 \ddot{\mathbf{x}}_{k-1} \tag{A.21}$$

Bibliography

[1] Xiaoyun Shao, Andrei M Reinhorn, and Mettupalayam V Sivaselvan. "Real-time hybrid simulation using shake tables and dynamic actuators". In: *Journal of Structural Engineering* 137.7 (2010), pp. 748–760.

[2] Motohiko Hakuno, Masatoshi Shidawara, and Tsukasa Hara. "Dynamic destructive test of a cantilever beam, controlled by an analog-computer". In: *Proceedings of the Japan Society of Civil Engineers.* Japan Society of Civil Engineers. 1969, pp. 1–9.

[3] Mikhail V Andreev, Alexandr S Gusev, Nikolay Yu Ruban, et al. "Hybrid real-time simulator of large-scale power systems". In: *IEEE Transactions on Power Systems* 34.2 (2019), pp. 1404–1415.

[4] Adit Joshi. "A Novel Approach for Validating Adaptive Cruise Control (ACC) Using Two Hardware-in-the-Loop (HIL) Simulation Benches". In: *SAE Technical Paper.* SAE International, Apr. 2019. DOI: 10.4271/2019-01-1038. URL: https://doi.org/10.4271/2019-01-1038.

[5] Masayoshi Nakashima, Hiroto Kato, and Eiji Takaoka. "Development of real-time pseudo dynamic testing". In: *Earthquake Engineering & Structural Dynamics* 21.1 (1992), pp. 79–92.

[6] Richard Christenson, Yi Zhong Lin, Andrew Emmons, et al. "Large-scale experimental verification of semiactive control through real-time hybrid simulation". In: *Journal of Structural Engineering* 134.4 (2008), pp. 522–534.

[7] Cheng Chen and James M Ricles. "Large-scale real-time hybrid simulation involving multiple experimental substructures and adaptive actuator delay compensation". In: *Earthquake Engineering & Structural Dynamics* 41.3 (2012), pp. 549–569.

[8] Yunbyeong Chae, James M Ricles, and Richard Sause. "Large-scale experimental studies of structural control algorithms for structures with magnetorheological dampers using real-time hybrid simulation". In: *Journal of Structural Engineering* 139.7 (2012), pp. 1215–1226.

[9] Yunbyeong Chae, Karim Kazemibidokhti, and James M Ricles. "Adaptive time series compensator for delay compensation of servo-hydraulic actuator systems for real-time hybrid simulation". In: *Earthquake Engineering & Structural Dynamics* 42.11 (2013), pp. 1697–1715.

[10] Oya Mercan and James M Ricles. "Experimental studies on real-time testing of structures with elastomeric dampers". In: *Journal of structural engineering* 135.9 (2009), pp. 1124–1133.

[11] Teng Wu and Wei Song. "Real-time aerodynamics hybrid simulation: Wind-induced effects on a reduced-scale building equipped with full-scale dampers". In: *Journal of Wind Engineering and Industrial Aerodynamics* 190 (2019), pp. 1–9.

[12] Zili Zhang, Biswajit Basu, and Søren RK Nielsen. "Real-time hybrid aeroelastic simulation of wind turbines with various types of full-scale tuned liquid dampers". In: *Wind Energy* 22.2 (2019), pp. 239–256.

[13] Thomas Sauder, Valentin Chabaud, Maxime Thys, et al. "Real-time hybrid model testing of a braceless semi-submersible wind turbine: Part I—The hybrid approach". In: *ASME 2016 35th International Conference on Ocean, Offshore and Arctic Engineering*. American Society of Mechanical Engineers. 2016, V006T09A039–V006T09A039.

[14] Stefan Arenfeldt Vilsen, T Sauder, Asgeir Johan Sørensen, et al. "Method for Real-Time Hybrid Model Testing of ocean structures: Case study on horizontal mooring systems". In: *Ocean Engineering* 172 (2019), pp. 46–58.

[15] Rolf Isermann, Jochen Schaffnit, and Stefan Sinsel. "Hardware-in-the-loop simulation for the design and testing of engine-control systems". In: *Control Engineering Practice* 7.5 (1999), pp. 643–653.

[16] Alain Bouscayrol. "Different types of hardware-in-the-loop simulation for electric drives". In: *Industrial Electronics, 2008. ISIE 2008. IEEE International Symposium on*. IEEE. 2008, pp. 2146–2151.

[17] Hosam K Fathy, Zoran S Filipi, Jonathan Hagena, et al. "Review of hardware-in-the-loop simulation and its prospects in the automotive area". In: *Modeling and simulation for military applications*. Vol. 6228. International Society for Optics and Photonics. 2006, 62280E.

[18]   Marko Bacic. "On hardware-in-the-loop simulation". In: *Decision and Control, 2005 and 2005 European Control Conference. CDC-ECC'05. 44th IEEE Conference on.* IEEE. 2005, pp. 3194–3198.

[19]   Kui Luo, Wenhui Shi, Yongning Chi, et al. "Stability and accuracy considerations in the design and implementation of wind turbine power hardware in the loop platform". In: *CSEE Journal of Power and Energy Systems* 3.2 (2017), pp. 167–175.

[20]   Saddam Aziz, Huaizhi Wang, Yitao Liu, et al. "Variable Universe Fuzzy Logic-Based Hybrid LFC Control With Real-Time Implementation". In: *IEEE Access* 7 (2019), pp. 25535–25546.

[21]   James Cale, Brian Johnson, Emiliano Dall'Anese, et al. "Mitigating Communication Delays in Remotely Connected Hardware-in-the-loop Experiments". In: *IEEE Transactions on Industrial Electronics* (2018).

[22]   Simiao Yu, Junwei Han, Zhiyong Qu, et al. "A Force and Displacement Compensation Method towards Divergence and Accuracy of Hardware-In-The-Loop Simulation System for Manipulator Docking". In: *IEEE Access* (2018).

[23]   Adit Joshi. *Hardware-in-the-Loop (HIL) Implementation and Validation of SAE Level 2 Autonomous Vehicle with Subsystem Fault Tolerant Fallback Performance for Takeover Scenarios.* Tech. rep. SAE Technical Paper, 2017.

[24]   Koichi Takanashi, Kuniaki Udagawa, Matsutaro Seki, et al. "Nonlinear earthquake response analysis of structures by a computer-actuator on-line system". In: *Bulletin of Earthquake Resistant Structure Research Center* 8 (1975), pp. 1–17.

[25]   Stephen A Mahin and Pui-shum B Shing. "Pseudodynamic method for seismic testing". In: *Journal of Structural Engineering* 111.7 (1985), pp. 1482–1503.

[26]   K Takanashi and K Ohi. "Earthquake response analysis of steel structures by rapid computer-actuator on-line system,(1) a progress report, trial system and dynamic response of steel beams". In: *Bull. Earthquake Resistant Struct. Research Center (ERS)* 16 (1983), pp. 103–109.

[27]   Stavros N Dermitzakis and Stephen A Mahin. "Development of substructuring techniques for on-line computer controlled seismic performance testing". PhD thesis. University of California, Berkeley, 1985.

[28] RP Dhakal, JB Mander, and N Mashiko. "Bidirectional pseudodynamic tests of bridge piers designed to different standards". In: *Journal of Bridge Engineering* 12.3 (2007), pp. 284–295.

[29] Makoto Obata and Yoshiaki Goto. "Development of multidirectional structural testing system applicable to pseudodynamic test". In: *Journal of Structural Engineering* 133.5 (2007), pp. 638–645.

[30] H Iemura, A Igarashi, and Y Takahashi. "Substructured hybrid techniques for actuator loading and shaking table tests". In: *Proceedings of the First International Conference on Advances in Structural Engineering and Mechanics*. 1999, pp. 821–826.

[31] Mariantonieta Gutierrez Soto and Hojjat Adeli. "Tuned mass dampers". In: *Archives of Computational Methods in Engineering* 20.4 (2013), pp. 419–431.

[32] Said Elias and Vasant Matsagar. "Research developments in vibration control of structures using passive tuned mass dampers". In: *Annual Reviews in Control* 44 (2017), pp. 129–156.

[33] Akira Igarashi, Hirokazu Iemura, and Takanori Suwa. "Development of substructured shaking table test method". In: *Proceedings of the 12th World Conference on Earthquake Engineering*. 2000.

[34] Andreas H Schellenberg, Tracy C Becker, and Stephen A Mahin. "Hybrid shake table testing method: Theory, implementation and application to midlevel isolation". In: *Structural Control and Health Monitoring* 24.5 (2017), e1915.

[35] Gaston A Fermandois and Billie F Spencer. "Model-based framework for multiaxial real-time hybrid simulation testing". In: *Earthquake Engineering and Engineering Vibration* 16.4 (2017), pp. 671–691.

[36] Joseph Colletti. "Enabling Full-Scale Soil-Structure Interaction Modeling through Analysis of a Geotechnical Laminar Box and Real-time Dynamic Hybrid Simulation". PhD thesis. State University of New York at Buffalo, 2019.

[37] Thomas Sauder. "Fidelity of Cyber-Physical Empirical Methods Application to the active truncation of slender marine structures". PhD thesis. Norwegian University of Science and Technology, 2018.

[38] Ali Irmak Ozdagli. "Distributed real-time hybrid simulation: Modeling, development and experimental validation". PhD thesis. Purdue University, 2015.

[39] Xin Li, Ali I Ozdagli, Shirley J Dyke, et al. "Development and Verification of Distributed Real-Time Hybrid Simulation Methods". In: *Journal of Computing in Civil Engineering* 31.4 (2017), p. 04017014.

[40] Li-Qiao Lu, Jin-Ting Wang, and Fei Zhu. "Improvement of Real-Time Hybrid Simulation Using Parallel Finite-Element Program". In: *Journal of Earthquake Engineering* (2018), pp. 1–19.

[41] SJ Dyke, BF Spencer Jr, P Quast, et al. "Role of control-structure interaction in protective system design". In: *Journal of Engineering Mechanics* 121.2 (1995), pp. 322–338.

[42] Amin Maghareh, Christian E Silva, and Shirley J Dyke. "Servo-hydraulic actuator in controllable canonical form: Identification and experimental validation". In: *Mechanical Systems and Signal Processing* 100 (2018), pp. 398–414.

[43] Christian E Silva, Daniel Gomez, Amin Maghareh, et al. "Benchmark control problem for real-time hybrid simulation". In: *Mechanical Systems and Signal Processing* 135 (2020), p. 106381.

[44] Juan E Carrion and Billie F Spencer Jr. *Model-based strategies for real-time hybrid testing*. Tech. rep. Newmark Structural Engineering Laboratory. University of Illinois at Urbana . . ., 2007.

[45] J Zhao, C French, C Shield, et al. "Considerations for the development of real-time dynamic testing using servo-hydraulic actuation". In: *Earthquake Engineering & Structural Dynamics* 32.11 (2003), pp. 1773–1794.

[46] Nakagawa M. Sugano M. Horiuchi T. and T. Konno. "Development of a Real-time Hybrid Experimental System with Actuator Delay Compensation". In: *In Proceedings of 11th World Conference in Earthquake Engineering, number 660, Acapulco, Mexico*. 1996.

[47] Amin Maghareh. "Nonlinear Robust Framework for Real-time Hybrid Simulation of Structural Systems: Design, Implementation, and Validation". PhD thesis. Purdue University, 2017.

[48] Amin Maghareh, Shirley J Dyke, Arun Prakash, et al. "Establishing a stability switch criterion for effective implementation of real-time hybrid simulation". In: *Smart Structures and Systems* 14.6 (2014), pp. 1221–1245.

[49] Xiuyu Gao, Nestor Castaneda, and Shirley J Dyke. "Real time hybrid simulation: from dynamic system, motion control to experimental error". In: *Earthquake Engineering & Structural Dynamics* 42.6 (2013), pp. 815–832.

[50] Xiuyu S Gao and Shawn You. "Dynamical stability analysis of MDOF real-time hybrid system". In: *Mechanical Systems and Signal Processing* 133 (2019), p. 106261.

[51] Amin Maghareh, Shirley J Dyke, Arun Prakash, et al. *Establishing Predictive Indicators for Stability and Performance of SDOF Real-time Hybrid Simulations*. Tech. rep. Technical Report, 2013.

[52] Amin Maghareh, Shirley J Dyke, Arun Prakash, et al. "Establishing a predictive performance indicator for real-time hybrid simulation". In: *Earthquake Engineering & Structural Dynamics* 43.15 (2014), pp. 2299–2318.

[53] Amin Maghareh, Shirley Dyke, Siamak Rabieniaharatbar, et al. "Predictive stability indicator: a novel approach to configuring a real-time hybrid simulation". In: *Earthquake Engineering & Structural Dynamics* 46.1 (2017), pp. 95–116.

[54] Richard Christenson, SJ Dyke, J Zhang, et al. "Hybrid simulation: a discussion of current assessment measures". In: *Purdue University* (2014).

[55] AP Darby, A Blakeborough, and MS Williams. "Real-time substructure tests using hydraulic actuator". In: *Journal of Engineering Mechanics* 125.10 (1999), pp. 1133–1139.

[56] T Horiuchi, M Inoue, T Konno, et al. "Real-time hybrid experimental system with actuator delay compensation and its application to a piping system with energy absorber". In: *Earthquake Engineering & Structural Dynamics* 28.10 (1999), pp. 1121–1141.

[57] AP Darby, A Blakeborough, and MS Williams. "Improved control algorithm for real-time substructure testing". In: *Earthquake engineering & structural dynamics* 30.3 (2001), pp. 431–448.

[58] Toshihiko Horiuchi and Takao Konno. "A new method for compensating actuator delay in real–time hybrid experiments". In: *Philosophical Transactions of the Royal Society of London A: Mathematical, Physical and Engineering Sciences* 359.1786 (2001), pp. 1893–1909.

[59] Bin Wu, Zhen Wang, and Oreste S Bursi. "Actuator dynamics compensation based on upper bound delay for real-time hybrid simulation". In: *Earthquake Engineering & Structural Dynamics* 42.12 (2013), pp. 1749–1765.

[60] Fei Zhu, Jin-Ting Wang, Feng Jin, et al. "Analysis of delay compensation in real-time dynamic hybrid testing with large integration time-step". In: *Smart Structures and Systems* 14.6 (2014), pp. 1269–1289.

[61] Yao Gui, Jin-Ting Wang, Feng Jin, et al. "Development of a family of explicit algorithms for structural dynamics with unconditional stability". In: *Nonlinear Dynamics* 77.4 (2014), pp. 1157–1170.

[62] Xizhan Ning, Zhen Wang, Huimeng Zhou, et al. "Robust actuator dynamics compensation method for real-time hybrid simulation". In: *Mechanical Systems and Signal Processing* 131 (2019), pp. 49–70.

[63] Huimeng Zhou, Dan Xu, Xiaoyun Shao, et al. "A robust linear-quadratic-gaussian controller for the real-time hybrid simulation on a benchmark problem". In: *Mechanical Systems and Signal Processing* 133 (2019), p. 106260.

[64] Rae-Young Jung, P Benson Shing, Eric Stauffer, et al. "Performance of a real-time pseudodynamic test system considering nonlinear structural response". In: *Earthquake Engineering & Structural Dynamics* 36.12 (2007), pp. 1785–1809.

[65] Brian M Phillips and Billie F Spencer Jr. *Model-based feedforward-feedback tracking control for real-time hybrid simulation.* Tech. rep. Newmark Structural Engineering Laboratory. University of Illinois at Urbana . . ., 2011.

[66] Brian M Phillips, Shuta Takada, BF Spencer Jr, et al. "Feedforward actuator controller development using the backward-difference method for real-time hybrid simulation". In: *Smart Structures and Systems* 14.6 (2014), pp. 1081–1103.

[67] Narutoshi Nakata and Matthew Stehman. "Compensation techniques for experimental errors in real-time hybrid simulation using shake tables". In: *Smart Structures and Systems* 14.6 (2014), pp. 1055–1079.

[68] Saeid Hayati and Wei Song. "Design and Performance Evaluation of an Optimal Discrete-Time Feedforward Controller for Servo-Hydraulic Compensation". In: *Journal of Engineering Mechanics* 144.2 (2017), p. 04017163.

[69] Ge Ou, Ali Irmak Ozdagli, Shirley J Dyke, et al. "Robust integrated actuator control: experimental verification and real-time hybrid-simulation implementation". In: *Earthquake Engineering & Structural Dynamics* 44.3 (2015), pp. 441–460.

[70] Rae-Young Jung and P Benson Shing. "Performance evaluation of a real-time pseudodynamic test system". In: *Earthquake engineering & structural dynamics* 35.7 (2006), pp. 789–810.

[71] PA Bonnet, CN Lim, MS Williams, et al. "Real-time hybrid experiments with Newmark integration, MCSmd outer-loop control and multi-tasking strategies". In: *Earthquake Engineering & Structural Dynamics* 36.1 (2007), pp. 119–141.

[72] Cheng Chen. *Development and numerical simulation of hybrid effective force testing method.* Lehigh University, 2007.

[73] Cheng Chen and James M Ricles. "Improving the inverse compensation method for real-time hybrid simulation through a dual compensation scheme". In: *Earthquake Engineering & Structural Dynamics* 38.10 (2009), pp. 1237–1255.

[74] X Shao and AM Reinhorn. "Development of a controller platform for force-based real-time hybrid simulation". In: *Journal of Earthquake Engineering* 16.2 (2012), pp. 274–295.

[75] Mohit Verma, J Rajasankar, and Nagesh R Iyer. "Fuzzy logic controller for real-time substructuring applications". In: *Journal of Vibration and Control* 20.8 (2014), pp. 1103–1118.

[76] Selim Günay and Khalid M Mosalam. "Enhancement of real-time hybrid simulation on a shaking table configuration with implementation of an advanced control method". In: *Earthquake Engineering & Structural Dynamics* 44.5 (2015), pp. 657–675.

[77] Matthew Stehman and Narutoshi Nakata. "IIR compensation in real-time hybrid simulation using shake tables with complex control-structure-interaction". In: *Journal of Earthquake Engineering* 20.4 (2016), pp. 633–653.

[78] Mohit Verma and MV Sivaselvan. "Impedance matching control design for the benchmark problem in real-time hybrid simulation". In: *Mechanical Systems and Signal Processing* 134 (2019), p. 106343.

[79] SA Neild, D Drury, and DP Stoten. "An improved substructuring control strategy based on the adaptive minimal control synthesis control algorithm". In: *Proceedings of the Institution of Mechanical Engineers, Part I: Journal of Systems and Control Engineering* 219.5 (2005), pp. 305–317.

[80] SA Neild, DP Stoten, D Drury, et al. "Control issues relating to real-time substructuring experiments using a shaking table". In: *Earthquake engineering & structural dynamics* 34.9 (2005), pp. 1171–1192.

[81] CN Lim, SA Neild, DP Stoten, et al. "Using adaptive control for dynamic substructuring tests". In: *Proc. of the 3rd European Conf. on Structural Control*. 2004.

[82] CN Lim, SA Neild, DP Stoten, et al. "Adaptive control strategy for dynamic substructuring tests". In: *Journal of Engineering Mechanics* 133.8 (2007), pp. 864–873.

[83] AP Darby, MS Williams, and A Blakeborough. "Stability and delay compensation for real-time substructure testing". In: *Journal of Engineering Mechanics* 128.12 (2002), pp. 1276–1284.

[84] M Ahmadizadeh, G Mosqueda, and AM Reinhorn. "Compensation of actuator delay and dynamics for real-time hybrid structural simulation". In: *Earthquake Engineering & Structural Dynamics* 37.1 (2008), pp. 21–42.

[85] MI Wallace, DJ Wagg, and SA Neild. "An adaptive polynomial based forward prediction algorithm for multi-actuator real-time dynamic substructuring". In: *Proceedings of the Royal Society A: Mathematical, Physical and Engineering Sciences* 461.2064 (2005), pp. 3807–3826.

[86] Jia-Ying Tu, Wei-De Hsiao, and Chih-Ying Chen. "Modelling and control issues of dynamically substructured systems: adaptive forward prediction taken as an example". In: *Proceedings of the Royal Society A: Mathematical, Physical and Engineering Sciences* 470.2168 (2014), p. 20130773.

[87] David J. Wagg Zhou Huimeng and Mengning Li. "Equivalent force control combined with adaptive polynomial-based forward prediction for real-time hybrid simulation". In: *Structural Control and Health Monitoring* 24.11 (2017).

[88] Bin Wu, Qianying Wang, P Benson Shing, et al. "Equivalent force control method for generalized real-time substructure testing with implicit integration". In: *Earthquake engineering & structural dynamics* 36.9 (2007), pp. 1127–1149.

[89] Dan Xu, Huimeng Zhou, Xiaoyun Shao, et al. "Performance study of sliding mode controller with improved adaptive polynomial-based forward prediction". In: *Mechanical Systems and Signal Processing* 133 (2019), p. 106263.

[90] Zhen Wang, Xizhan Ning, Guoshan Xu, et al. "High performance compensation using an adaptive strategy for real-time hybrid simulation". In: *Mechanical Systems and Signal Processing* 133 (2019), p. 106262.

[91] Pei-Ching Chen and Keh-Chyuan Tsai. "Dual compensation strategy for real-time hybrid testing". In: *Earthquake Engineering & Structural Dynamics* 42.1 (2013), pp. 1–23.

[92] Junjie Tao and Oya Mercan. "A study on a benchmark control problem for real-time hybrid simulation with a tracking error-based adaptive compensator combined with a supplementary proportional-integral-derivative controller". In: *Mechanical Systems and Signal Processing* 134 (2019), p. 106346.

[93] Cheng Chen and James M Ricles. "Tracking error-based servohydraulic actuator adaptive compensation for real-time hybrid simulation". In: *Journal of Structural Engineering* 136.4 (2010), pp. 432–440.

[94] Oya Mercan. *Analytical and experimental studies on large scale, real-time pseudodynamic testing*. Lehigh University, 2007.

[95] Cheng Chen, James M Ricles, and Tong Guo. "Improved adaptive inverse compensation technique for real-time hybrid simulation". In: *Journal of Engineering Mechanics* 138.12 (2012), pp. 1432–1446.

[96] Weijie Xu, Cheng Chen, Tong Guo, et al. "Evaluation of frequency evaluation index based compensation for benchmark study in real-time hybrid simulation". In: *Mechanical Systems and Signal Processing* 130 (2019), pp. 649–663.

[97] Yunbyeong Chae, Ramin Rabiee, Abdullah Dursun, et al. "Real-time force control for servo-hydraulic actuator systems using adaptive time series compensator and compliance springs". In: *Earthquake Engineering & Structural Dynamics* 47.4 (2018), pp. 854–871.

[98] Alejandro Palacio-Betancur and Mariantonieta Gutierrez Soto. "Adaptive tracking control for real-time hybrid simulation of structures subjected to seismic loading". In: *Mechanical Systems and Signal Processing* 134 (2019), p. 106345.

[99] Pei-Ching Chen, Chia-Ming Chang, Billie F Spencer, et al. "Adaptive model-based tracking control for real-time hybrid simulation". In: *Bulletin of Earthquake Engineering* 13.6 (2015), pp. 1633–1653.

[100] Yuting Ouyang, Weixing Shi, Jiazeng Shan, et al. "Backstepping adaptive control for real-time hybrid simulation including servo-hydraulic dynamics". In: *Mechanical Systems and Signal Processing* 130 (2019), pp. 732–754.

[101] Amin Maghareh, Shirley J Dyke, and Christian E Silva. "A Self-tuning Robust Control System for nonlinear real-time hybrid simulation". In: *Earthquake Engineering & Structural Dynamics* 49.7 (2020), pp. 695–715.

[102] Masayoshi Nakashima and Nobuaki Masaoka. "Real-time on-line test for MDOF systems". In: *Earthquake engineering & structural dynamics* 28.4 (1999), pp. 393–420.

[103] Cheng Chen, James M Ricles, Thomas M Marullo, et al. "Real-time hybrid testing using the unconditionally stable explicit CR integration algorithm". In: *Earthquake Engineering & Structural Dynamics* 38.1 (2009), pp. 23–44.

[104] Pei-Ching Chen, Keh-Chyuan Tsai, and Pei-Yang Lin. "Real-time hybrid testing of a smart base isolation system". In: *Earthquake Engineering & Structural Dynamics* 43.1 (2014), pp. 139–158.

[105] Xiuyu Gao. "Development of a robust framework for real-time hybrid simulation: From dynamical system, motion control to experimental error verification". PhD thesis. Purdue University, 2012.

[106] Kiyoshi Kanai. "Semi-empirical formula for the seismic characteristics of the ground". In: *Bulletin of the earthquake research institute* 35 (1957), pp. 309–325.

[107] Hiroshi Tajimi. "A statistical method of determing the maximum response of a building structure during an earthquake." In: *Proc. 2nd World Conf. Earthq. Eng.* 1960, pp. 781–797.

[108] Chunxiang Li and Yanxia Liu. "Ground motion dominant frequency effect on the design of multiple tuned mass dampers". In: *Journal of earthquake engineering* 8.01 (2004), pp. 89–105.

[109] Genda Chen and Jingning Wu. "Optimal placement of multiple tune mass dampers for seismic structures". In: *Journal of Structural Engineering* 127.9 (2001), pp. 1054–1062.

[110] Mariantonieta Gutierrez Soto and Hojjat Adeli. "Multi-agent replicator controller for sustainable vibration control of smart structures". In: *Journal of Vibroengineering* 19 (2017), pp. 4300–4322.

[111] Nam Hoang, Yozo Fujino, and Pennung Warnitchai. "Optimal tuned mass damper for seismic applications and practical design formulas". In: *Engineering Structures* 30.3 (2008), pp. 707–715.

[112] PA Bonnet, MS Williams, and A Blakeborough. "Evaluation of numerical time-integration schemes for real-time hybrid testing". In: *Earthquake engineering & structural dynamics* 37.13 (2008), pp. 1467–1490.

[113] Jinting Wang, Liqiao Lu, and Fei Zhu. "Efficiency analysis of numerical integrations for finite element substructure in real-time hybrid simulation". In: *Earthquake Engineering and Engineering Vibration* 17.1 (2018), pp. 73–86.

[114] Shuenn-Yih Chang. "Explicit pseudodynamic algorithm with unconditional stability". In: *Journal of Engineering Mechanics* 128.9 (2002), pp. 935–947.

[115] Cheng Chen and James M Ricles. "Stability analysis of SDOF real-time hybrid testing systems with explicit integration algorithms and actuator delay". In: *Earthquake Engineering & Structural Dynamics* 37.4 (2008), pp. 597–613.

[116] Chinmoy Kolay and James M Ricles. "Development of a family of unconditionally stable explicit direct integration algorithms with controllable numerical energy dissipation". In: *Earthquake Engineering & Structural Dynamics* 43.9 (2014), pp. 1361–1380.

[117] Yu Tang and Menglin Lou. "New unconditionally stable explicit integration algorithm for real-time hybrid testing". In: *Journal of Engineering Mechanics* 143.7 (2017), p. 04017029.

Alejandro Palacio Betancur, BSc

EDUCATION

Bachelor of Science, Civil Engineering August 2016
Universidad Nacional de Colombia, Medellin, Colombia GPA 3.86/4.0
Thesis: "Statics, stability and vibration of non-prismatic beams and column with finite generalized end conditions" - Advisor: Dr. Jose Dario Aristizabal-Ochoa

PROFESSIONAL APPOINTMENTS

2018 - Present Graduate Research Assistant, University of Kentucky
2018 - 2018 Structural Civil Engineer Junior, Integral S.A. Consulting Engineers
2015 - 2018 Undergraduate Research Assistant, Universidad Nacional de Colombia

SUMMARY OF SCHOLARLY ACTIVITY

- Google scholar
- 3 first-author journal publications

JOURNAL PUBLICATIONS

1. **Palacio-Betancur, A.** and Aristizabal-Ochoa J.D. (2018) "Second-order Stiffness Matrix and Loading Vector of a Tapered Rectangular Timoshenko Beam-column With Semirigid Connections" *Structures* 15: 221-223 DOI: 10.1016/j.istruc.
2018.07.002

2. **Palacio-Betancur, A.** and Aristizabal-Ochoa J.D. (2019) "Statics, stability and vibration of non-prismatic linear beam-columns with semirigid connections on elastic foundation" *Engineering Structures* 181: 89-94 DOI: 10.1016/j.engstruct.2018.12.
002

3. **Palacio-Betancur, A.** and M. Gutierrez Soto (2019) "Adaptive tracking control for real-time hybrid simulation of structures subjected to seismic loading" *Mechanical Systems and Signal Processing* 134: 106345. DOI: 10.1016/j.ymssp.2019.106345

4. **Palacio-Betancur, A.** and M. Gutierrez Soto "Real-Time Hybrid Simulation of Civil Engineering Structures: A State-of-the-art Review" (In Preparation - Draft available upon request)

CONFERENCE PRESENTATIONS

1. **A. Palacio-Betancur** and M. Gutierrez Soto "Numerical Integration Methods for Real-Time Hybrid Simulation of Structures Subjected to Earthquake Loading" *Engineering Mechanics Institute Conference* June 18, 2019. Pasadena, CA.

2. **A. Palacio-Betancur** and M. Gutierrez Soto "Multi-objective optimization of actuator and sensor location of diagrid structures subjected to earthquake loading" *International Workshop on Advanced Smart Materials and Smart Structures Technology* July 19, 2019. Rome, Italy.

3. **A. Palacio-Betancur** and M. Gutierrez Soto "Application of multi-axial Real-time Hybrid Simulation (maRTHS) using small-scale shake tables for research

and education" *Engineering Mechanics Institute Conference* May 26, 2020. New York, NY.

4. **A. Palacio-Betancur** and M. Gutierrez Soto "Hybrid counter propagation neural dynamic model for structural design optimization of diagrid structures" 17th *World Conference on Earthquake Engineering* September 18, 2020. Sendai, Japan.

5. **A. Palacio-Betancur** and M. Gutierrez Soto "Structural design optimization for vibration control of diagrid structures using a neural dynamic model" 17th *World Conference on Earthquake Engineering* September 18, 2020. Sendai, Japan.

HONORS AND AWARDS

Third place at the Timber-Strong Design Build Competition
NCSEA Structural Engineering Summit, Disneyland Hotel
Anaheim, CA   2019
    Asia-Pacific-Euro Summer School 2019 Group Competition 1st classified
Sapienza, University of Rome
Rome, Italy   2019
    Initiate of the College of Civil Engineering's Honors Society Chi Epsilon
University of Kentucky
Lexington, KY   2019
    Graduate student among the best 10% academic grade average in undergraduate Civil Engineering.
Universidad Nacional de Colombia
Medellín, Colombia   2016